Aus der Klinik für Neurologie
der Medizinischen Fakultät Charité – Universitätsmedizin Berlin

DISSERTATION

Bandwidth-Specific Functional Connectivity of Physiological Low Frequency Oscillations in fMRI

zur Erlangung des akademischen Grades
Doctor medicinae (Dr. med.)

vorgelegt der Medizinischen Fakultät
Charité – Universitätsmedizin Berlin

von

Sein H. Schmidt

aus Southfield MI (USA)

Gutachter: 1. Herr PD Dr. med. H. Obrig

2. Herr Prof. M. Kohl-Bareis

3. Herr Prof. Dr. med. KT. Hoffmann

Datum der Promotion: 2. Februar 2009

Abstract:

With over forty publications on resting state connectivity in functional magnetic resonance imaging (fMRI) and over fifty years of invasive research in animals, the origin of various low frequency oscillatory states remains unresolved. Here the question will be answered: Is it possible to differentiate functional connectivity into two bandwidths, i.e. at very low and low frequencies? If it is possible to differentiate two bandwidths in fMRI resting state connectivity, then a connection to investigations from other modalities with well-defined physiological and pathological relevance can be established. A review of previous literature suggests that low frequency oscillations dominate in “very low frequencies” rather than in “low frequencies”, i.e. 0.04 Hz versus 0.08 Hz. Further, it is plausible that both bandwidths co-exist independent of each other, have a neural origin, and are independent of cerebral vasomotion as well as cardiac and respiratory cycles. We apply a hybrid fMRI approach to investigate the resting state with selectively filtered seed-voxels from the dominant primary motor cortex. We find, with both spectral and time-domain analyses, connectivity between segregated distant areas of the brain. We conclude that functional connectivity in the resting state can be defined for both bandwidths. We argue that spectral analyses might be better equipped for their identification and that very low frequencies are more closely related to cerebral autoregulatory effects as compared e.g. to investigations of intracranial pressure and blood volume fluctuations in physiological and pathological settings.

Keywords:

Connectivity, Low frequency oscillations, Autoregulation, Neuroimaging, Cranial Pressure, Cerebral Blood Flow

Table of contents

Dedicated to my children Joëlle, Stevo, Keanus and Fabian, my wife Silvia, my Parents and Grandparents

Abbreviation listing

aBP	arterial Blood Pressure
BOLD	Blood Oxygen Level Dependent
CBV	Cerebral Blood Volume
CPP	Cerebral Perfusion Pressure
cpm	cycles per minute
DSP	Digital Signal Processing
EEG	Electroencephalography
fMRI	Functional Magnetic Resonance Imaging
HFO	High Frequency Oscillations
HHFO	High High Frequency Oscillations
ICP	Intracranial Pressure
LDF	Laser Doppler Flowmetry
LFFC	Low Frequency Functional Connectivity
LFO	Low Frequency Oscillations
M1	Primary motor cortex
NIRS	Near Infra-Red Spectroscopy
$_P02$	Partial Pressure of Oxygen
ROI	Region of Interest
RTC	ROI time course
SPM	Statistical Parametric Mapping
TCD	Transcranial Doppler Sonography
VVLFO	Very Very Low Frequency Oscillations
VLFO	Very Low Frequency Oscillations

1 Introduction

The purpose of this dissertation is the investigation of low frequency cerebral oscillations in the healthy human adult brain as measured by functional resonance imaging (fMRI), a noninvasive tool to investigate cortical hemodynamics. The goal is to explore their functional connectivity in resting state data.

1.1 LFO and VLFO

Classically, low frequency oscillations of cerebral circulation have been defined below 0.1 Hz. More recently, it has been suggested that these low frequency oscillations can be differentiated in a "low frequency" bandwidth (0.05-0.1 Hz, here defined as "LFO") and a "very low frequency" bandwidth (0.015-0.05 Hz, here defined as "VLFO"). Their differential contribution to low frequency functional connectivity is unknown and has not been previously investigated. On the other hand, in the last years multiple fMRI Projects (see Table 3 and 4) have successfully investigated resting state connectivity in the human with fMRI in both healthy subjects and patients with various diseases. The origin of these fluctuations is uncertain and the bandwidths and terminology remain confusing.

1.1.1 Low frequency oscillations in animal research

Classic investigation of cerebral circulation began as early as the 1850's with transparent windows inserted into the skulls of animals. Davies and Bronk first recorded spontaneous low frequency fluctuations in cerebral oxygen supply in 1957[1]. They were confirmed in further investigations[2-6], have been found in NADH[7], cytochrome oxidase[8], laser-Doppler flowmetry (LDF)[9,10] and reflectance oximetry[11] as well as in the human with LDF[12,13], Near Infra-Red Spectroscopy (NIRS)[14,15] and functional Magnetic Resonance Imaging (fMRI) [16]. Their origin has been discussed in terms of cerebral autoregulation[17,18], or of neurovascular origin in which fluctuations are part of a general arousal system[19,20], of a complex system[21] or as a carrier for long-distance information processing of higher frequencies[22]. Although the etiology remains unclear the phenomena is beyond doubt: "A striking feature of these investigations in man is their fluctuation nature"[23].

Cerebral autoregulation is defined as the *orthostatic* maintenance of cerebral blood flow (CBF= 50 milliliters (ml) of blood per 100 grams (g) of brain tissue per minute) in the face of changes of arterial pressure[18]. Or more explicitly, it reflects independence of the cerebral blood flow and circulatory-metabolic supply of cerebral activity from cerebral hemodynamics[24]. In general, it is thought to be directly linked to vasomotion[25]. Here, smooth muscle produces coherent waves over long distance of the vessel, possibly to reduce the resistance in CBF.

Others argue that low frequency oscillations have a neural origin due to a tight neurovascular coupling. Low frequency oscillation arise when brain electric activity is depressed[6,7]. They appear independent of each other, even when they are measured only a few millimeters apart[26,27]. During stimulation their correlation can go from <50% to 80% within a short period of time[28]. They co-vary with electroencephalography (EEG) fluctuations[29], are suspended by hyperemia, i.e. by hypercapnia and halothane in low doses and are produced by hypoxemia[18,30], e.g. hypotension, hyperventilation, cerebral artery occlusion and vasoconstriction. These observations challenge the theory of vasomotor origin[18].

Modulation	CBF	O2 availability	Fluctuations	Vasomotion
Hyperpnoea	--[1]	--[1]		
Hypercapnia			cease (>2%)[1,7]	
Hypoxia	-/+[1]	--	++[1], cease[5,6,7]	
Hyperoxia	+/-[1]	++[1]		--[3]
Visual Stimulation	+[1]	++[1]		
Electric Stimulation	++[1]	++[1]		
Posture Change	--[1]	+/-[1]		
Anesthesia*			++[5]	
Hypothermia			++[5,9]	
Halothane/NO			cease[7]	
NO inhibitors			++[8]	
Vascular-Occlusion			ipsi --, contra ++[8]	

Table 1: Modulations of physiological oscillations: In the first column, the type of modulation is described. The following columns depict positive or negative deflection of the relative parameter. CBF: cerebral blood flow[131, 218, 332, 57, 7, 18, 33, 6.]

1.1.2 Low frequency oscillations in human research

Rhythmic oscillations in the human at low frequencies below the heart rate were first described during arterial blood pressure (ABP) monitoring by Hering, Traube, and Mayer as early as the 19th century. These phenomena have also been discussed in terms of Mayer, B- and C-waves as well as the V-signal.

Traube-Hering-Mayer waves (Syn.: M-Waves) are defined as rhythmical variations in blood pressure, usually extending over several respiratory cycles, with a frequency varying from *6 to 10 cpm,* related to variations in vasomotor tone. Simultaneous recordings of sympathetic nerve activity and arterial blood pressure have shown that the M waves of the systemic arterial blood pressure correlate with discharges of sympathetic neurons, which in turn account for the cerebral blood flow volume (CBFV) variations in the cerebral vasculature. They are usually considered to be associated with vasomotion[34].

B-waves were first described by Lundberg[35]. They are defined as non–heart-beat–related, slow and rhythmic oscillations in the intracranial pressure (ICP), with 0.5 to 2 cpm with pressure amplitudes from near indiscernible up to 50 mm Hg[36]. The physiological mechanisms behind the B-waves are still obscure[32,37,38,39]. They are frequent in hydrocephalus[40,41,] but are also reported in healthy individuals[42]. They were first attributed to the Cheyne-Stokes respiration of nonintubated patients with concomitant CO_2 partial pressure (PCO_2) fluctuations[35]. Since then they were also observed in ventilated patients with a steady pCO_2. Einhäupl and Venes postulated an autonomic (brain stem) rhythm as the pacemaker of intracranial pressure as well as cardiovascular fluctuations[43]. Magnæse postulated that B-waves were generated by changes in intracranial blood volume reflecting brain autoregulation[44]. In 1983, Rosner and Becker postulated an autoregulatory response of the cerebral vessels due to fluctuations of intracranial volume due to fluctuations of cerebral perfusion pressure (CPP) that evoked ICP oscillations[45] .

The distinction between B-waves with a frequency of 0.5–2 cpm and C-waves with a range of 4–8 cpm has been introduced by[35], yet the significance is unclear[46].

M-, B- and C-waves must be differentiated from respiratory oscillations (R-Waves) with 9-20 cpm. A clear correlation has been described for M-waves and R-waves between CBFV and arterial blood pressure (aBP). The results from these data were consistent with a high

pass filter model of cerebral autoregulation but also suggested that the principle of frequency-dependent vascular input impedances has to be considered in addition to autoregulatory feedback mechanisms. Further, unclear rhythmic slow fluctuations with various low frequency bandwidths have been observed in cerebral flow volume[47,48,] cerebral hemoglobin oxygenation in the jugular bulb[49], in brain tissue PO_2, as well as in cortical cytochrome oxidase and cortical blood volume (CBV).

In summary, VLFO might be analogous to B- and/or C-waves and LFO to M-waves. Thus, LFO would have a stronger association with aBP oscillations and sympatic function, whereas the origin of VLFO could be argued to be more closely related to synchronized “low frequency oscillations” in functional cerebral systems, i.e. functional connectivity.

Physiological oscillations	[cpm]	Definition	Method	Measure
B-waves	0.5 to 2	Spontaneous rhythmic oscillations in the intracranial pressure (autonomic brain stem rhythm, brain autoregulation, autoregulation of cerebral vessels	transcranial Doppler sonography, reflectance spectroscopy	CBF, ICP Oxidase, pO2, CBV
C-waves	4 to 8			
V-signal (Vasomotion)	~ 6	spontaneous, rhythmical contractions generated in many different types of smooth muscle	Optical imaging in the rat	CBF
Traube-Mayer Waves	6 to 10	Spontaneous rhythmical variations in blood pressure related to variations in vasomotor tone		aBP
M-Waves (Mayer Waves)	3 to 9	Spontaneous oscillations of blood pressure, heart rate, and cerebral blood flow velocities	transcranial Doppler sonography	1. correlate with discharges of sympathetic neurons 2. coherent with CBFV and aBP
R-waves (Respiratory Waves)	9 to 20	Spontaneous oscillations of blood pressure, heart rate, and cerebral blood flow velocities	transcranial Doppler sonography	Coherent with CBFV and aBP (thus cerebral autoregulation likely)

Table 2: Physiological oscillations in humans: In the first column, the physiological oscillations are listed. The following columns depict relevant parameters investigated. CBV: Cerebral blood volume, CBFV: cerebral blood flow volume, aBP: arterial blood pressure.

1.1.3 Low frequency oscillations in human research (fMRI)

Functional magnetic resonance (fMRI) allows for the simultaneous quantification of changes of blood oxygen dependent (BOLD) metabolic activity in local as well as distant regions of the brain. If multiple circumscribed regions of the brain show significant concurrent change in metabolic activity, then one can investigate not only these regions individually (segregated effects) but also the spatial and temporal characteristics of concurrent change for all regions in unison (integrated effects). If these changes are confined to functional networks of the brain, then they must be of neural origin. Thus, the question arises if low frequency fluctuations are functionally integrated phenomena? If so, then their neuro-vascular coupling must have a neural origin. If not, e.g. they are purely an effect of vasomotion than one would expect segregation related to cerebral vasculature. This is not the case. More than 30 fMRI studies show that various functional networks can be differentiated by LFO's. Most importantly, blind source separation allowed for the simultaneous identification of five functional systems[50]. In addition, asymmetrical connectivity in the Language Network ascertains that connectivity is not merely a spurious correlation of symmetrical effects of cerebral vascularization. Strong evidence exists that low frequency spatial modes can be differentiated cerebral systems, which implies some form of vascular-neural connection (see Table 3 and 4).

No previous investigations have discussed the differentiation of VLFO and LFO bandwidths in terms of functional connectivity. In the human, since Biswal and his colleague's first investigations in BOLD-fMRI, it has been generally accepted that the oscillations are defined in bandwidths below 0.1 Hz, and probably dominantly around 0.08 Hz[51]. However, most of the publications provide evidence that the dominant bandwidth is in the VLFO domain[52-60]. Of these, some deserve special mention[61,62,55]. They discuss the spectral characteristics of the fMRI signal. The first publication that addressed bandwidths of spectral information in functional connectivity decomposed the seed voxels correlation coefficient into spatial maps of specific bandwidths (0 - 0.1, 0.1 – 0.5 and 0.6 – 1.1 Hz), compared these with a localizer tasks and introduced null statistics via phase randomization. They found that the cross-correlation values of functional systems were highest for frequencies below 0.1 Hz. In contrast, the bandwidths of the ventricles were

non-specific; the arteries were dominated by “high-frequencies” (0.6 – 1.1 Hz) and the venous system by mid and to lesser extent low frequencies. Aliasing, found in CSF, was not present in the functional systems[63]. Strik et al. discussed the correlates of C- and B-waves, as well as respiratory and cardiac cycles in fMRI. Their results focused on cerebral fluid fluctuations, e.g. ventricle fluctuations. They found the ventricles dominated by all four factors, the basal artery by cardiac and respiratory frequencies, the sagittal venous system by C- and B-waves and functional parenchyma as relatively equipotent[64]. Beckmann and colleagues utilized a blind-source separation algorithm (probabilistic Independent Component Analysis, pICA), sampled at an adequate frequency (TR 124 ms) to avoid effects of aliasing. Their results provide evidence that at an adequate sampling rate the multiple functional systems with a dominant bandwidth of about 0.08 Hz can be found. Interestingly, in a later publication the dominant bandwidth was also 0.03 Hz[65,66].

In summary, independent statistical maps of low frequency connectivity can be found in VLFO and LFO bandwidths of resting state fMRI. These can be clearly differentiated from CSF as well as cardiac and respiratory fluctuations. Multiple functional systems can be differentiated. This is not due to aliasing. Thus, we suggest that these two forms of connectivity co-exist independently. They have a neurovascular correlate, which is reflected in well-known oscillatory phenomena found in TCD and ICP studies.

Authors	Ref.	Species	Technique	Parameter	VLFO [s^{-1}]	LFO [s^{-1}]	HFO [s^{-1}]	Magn.	Modulation	Remarks
Kleinfeldt	1995	rat	2-Photon microsc.	RBCv		~0.1				Cohere for <0.1 Hz
Biswal	1996	rat	Video-microscopy	RBCv		0.07–0.2			L-NAME	
Dirnagl	1993	rat	LDF	CBFv		0.1–0.18		18%	NOS-inhibitor	
Golanov	1996	rat	LDF	CBFv		~0.1		20%	Spontaneous	
Golanov	1994	rat	LDF	CBFv	~0.1		20%	Anesthesia	evoked by identified neurons	Synchron. across brain
Hudetz	1995	rat	LDF	CBFv		0.11–0.13		10%	L-NAME, CO2, anaesth.	
Hudetz	1992	rat	LDF	CBFv		0.07–0.18		14–30%	RR, CO2	
Morita	1992	rat	LDF	CBFv		0.08–0.17		5–10%	RR, U-shaped depencence	Frequency shifts by RR
Dora	1981	cat	Fluororeflectometer	NAD/H, CBV	0.03–0.05	0.08–0.17				Lag of NADH
Mayevsky	1991	rat	Fluororeflect./LDF	NAD/H, CBV, CBFV		0.1–0.15			CO2,O2	Ischemia related
Vern	1988	cat	Reflect.-spectrosc.	CYT, CBV		~0.15			No by sleep	Indep. metab./ vasc.
Vern	1997	rabbit	Reflect.-spectrosc.	CYT, *CBV*		<0.5 ~0.1		2–5%*3 5□	Stimulation?	Connectivity Phase shift HbO2-Cyt
Mayhew	1999	rat	Spectrosc. imaging	*HbO2, Cyt*				stim.*1*3		
Mayhew	1996	rat/cat	Spectrosc. imaging	Intrinsic signal		~0.1		1–2%	Stimulation?	Temp/spat inhomogen.
Cooper	1966	human	Polarogr. electr.	Invasive: pO2		~0.1		220%	Hypercapnia	Spatial inhomogen.
Livera	1992	neonate	NIRS	tot-Hb		0.05–0.08		(~3 mM)	Pathology?	
Chance	1993	human	NIRS NIRS	Absorption		0.1–5	~0.2	0.4 mM*2*3	Stimulation?	
Ebwell	1996	human		*oxy-*, deoxy- & tot-Hb						
Ebwell	1999	human	NIRS	*oxy-*, deoxy-& tot-Hb		0.08	0.22	0.6 mM*2*3		
Hoshi	1998/7	human	NIRS	oxy-, deoxy-& tot-Hb	0.01	0.08				
Diehl	1991/5	human	TCD	MCA-Fv	0.007	0.15		230%	Phase by ICA occlusion	Phase shift RR- LFO
Giller	1999	human	TCD	MCA-FI	0.006–0.037			7.5%		
Hu	1999	human	TCD	MCA-Fv	0.016–0.04	0.04–0.15	0.15–0.4		Phase/magn. by ICA occlusion	C test orr. with CO2-
Kuo	1998	human	TCD	MCA-Fv	0.016–0.04	0.04–0.15	0.15–0.4			Phase aBP-Fv
Zhang	1998	human	TCD	MCA-Fv	<0.07	~0.1	~0.2		Cerbral vasculature	
Zhang	1998	human	TCD	MCA-Fv	0.02–0.07	0.07–0.2	0.2–0.3	Orthostatic stress	functions as high pass filter	Indicator of autoreg.
Ba¨ zner	1995	human	TCD	MCA-Fv	0.01–0.05	0.05–0.15	0.15–0.5		Large/small artery disease	
Blaber	1997	human	TCD	MCA-Fv	~0.03	~0.1	~0.2		Orthostatic stress	Autoreg. high pass filter
Mitra	1997	human	BOLD-fMRI	BOLD-contrast		~0.1				Temp/spat inhomogen.
Biswal	1997	human	BOLD-fMRI	BOLD-contrast	~0.02	(~0.14)			Hypercapnia	Connectivity
Biswal	1995	human	BOLD-fMRI	BOLD-contrast		<0.08				Connectivity
Lowe	1998	human	BOLD-fMRI	BOLD-contrast		<0.08				Connectivity
Li	2000	human	BOLD-fMRI	contrast	~0.04	(~0.1)	~0.23		Cocaine	Connectivity

Table 3: Selection of Articles on Spontaneous Low Frequency Oscillations of Cerebral Blood Flow and Metabolism. The relevant parameters are listed in the column headings. The rows depict the publication. Table 3 reproduced with kind permission of the authors[67]. Table 4 with an emphasis on newer fMRI publications.

Authors	Year	Techn	Modulation	System	VLFO [s^{-1}]	LFO [s^{-1}]
Biswal	1995	fMRI	Hypercapnia	Motor,? aud. Vis?	0.02 (lt beckmann)	<0.08
Biswal	1997	fMRI		Motor	~0.02	(~0.14)
Mitra	1997	fMRI			~0.02	~0.1
Lowe	1998	fMRI		Vis, Amygdal, Motor	n.A	<0.08
Xiong	1999	fMRI	Hypercapnia	motor	< 0.1 Hz	< 0.1 Hz
Obrig	2000	NIRS		vis	0.02	0.1
Arfanakis	2000	fMRI		motor, vis, aud	0.03!	0.09
Cordes	2000	fMRI	anaesthesie	Motor, Visual, Auditory, Prefrontal	0.03!	0.06 (1/f)
Kiviniemi	2000	fMRI	cocain			
Li	2000	fMRI	n.a.	?	n.A	n.a.
Stein	2000	fMRI	Lesion	thalamus, hippocampus	<0.08	< 0.08
Quigley	2001	fMRI	n.a.	Speech, Aud. Motor	<0.1	<0.1
Cordes	2001	fMRI	MS			<0.1
Lowe	2002	fMRI		motor	< 0.08	< 0.08
Li	2002	fMRI		Hippocampus	n.a.	n.a.
Koch	2002	fMRI		U-fasern	< 0.8	< 0.8
Cordes	2002	fMRI	n.a.	visu,aud.motor.frontal.fusiform	0.03-0.1	0.03-0.1
Strik	2002	fMRI			0.008 – 0.05	(0.05-0.15)
Hampson	2002	fMRI	agenisis corpus callosum	Language (asymmetric)	< 0.1	< 0.1
Quigley	2003	fMRI		auditory, motor	n.a.	n.a.
Young	2003	PET		3a,3b,1,2	n.a.	n.a.
Peltier	2003	fMRI	anaesthesie	motor	< 0.1	< 0.1
Kiviniemi	2003	fMRI		vis, motor, aud	n.a.	n.a.
Greicius	2003	fMRI	n.a.	default mode	0.0083 - 0.15	0.0083 - 0.15
Rombouts	2003	fMRI		Hippocampus	0.03	n.a.
Sun	2004	fMRI	alzheimer	motor	0-0.15	0-0.15
Greicius	2004	fMRI		default mode	n.a.	n.a.
Van den Ven	2004	fMRI	motiion	sensorimotor, auditor, frontal	~0.04	0.08
Hampson	2004	fMRI	fingertap	V5, visual system	n.a.	n.a.
Sun	2005	fMRI	antidepressant(?), happy faces (?)	motor	0 - 0.15	0 - 0.15
Anand	2005	fMRI		depression, mood	< 0.08	< 0.08
Beckmann	2005	fMRI		Sensorimotor	0.02 (	0.08
Salvador	2005	fMRI			0.0004, 0.1518	0.0004, 0.1518
DeLuca	2006	fMRI		RSN 1-5	0.02	0.08
Nir	2006	fMRI	learning	PPA,IPC (visual system)	0.03	0.06
Sun	2006	fMRI		motor learning	s.o.	s.o.
Thirion	2006	fMRI		occip., parietal, parietofrontal	0.02-0.04	0,06

Table 4: Selection of Articles on Spontaneous Low Frequency Oscillations of Cerebral Blood Flow and Metabolism. The relevant parameters are listed in the column headings. The rows depict the publication. This table emphasizes recent publications in fMRI. It is not exhaustive, but aims to give an insight into the multiple bandwidths found in various systems and pathologies

1.2 Problem definition / State of research:

Slow oscillations of cerebral hemodynamics and metabolism have been studied by different techniques and in various species. Their origin is unclear; their frequency spectrum is ill defined. In addition, the terminology is confusing. Vasomotion or V-signal, Traube-Mayer, Mayer- or M-waves, B-waves, C-waves as well as spontaneous oscillations, and low frequency waves are used interchangeably and often synonymously (see Tables 2, 3 and 4). In addition, the following features are common to the phenomena described. They occur without overt stimulus (spontaneity). They can be differentiated form other respiratory and cardiac cycles (slowness). Moreover, they are altered by pharmacological and pathological conditions (modulatability).

These oscillations raise interest for three reasons: (1) Functional connectivity maps have been reported on their basis; (2) transcranial doppler (TCD) studies have shown that their phase relation to arterial blood pressure oscillations may reveal autoregulatory mechanisms of the brain vasculature; (3) alterations due to pathological conditions have been shown in human pathologies as well as a rat stroke model.

Little is known about their origin, yet it is important to elucidate their spatial and frequency characteristics for both normal physiological conditions and in those that may reflect brain injury or pathologies of diagnostic or prognostic value[18].

This work is not directly aimed at revealing the mechanisms underlying low frequency oscillations. They might be of vasomotor origin or reflect auto-regulation in physiological as well as in pathological settings. Indirect evidence will be presented that supports the notion of neurovascular coupling of neural origin; in contrast to vasomotion. Second, that in line with previous investigations from other modalities that oscillations can be found in two different distinct phase-locked bandwidths; e.g. VLFO and LFO in line with previous invasive animal and TCD or intracranial human investigations.

.

1.3 Direction of the argumentation

Recent findings in blood oxygen contrast dependent (BOLD) functional magnetic resonance imaging (fMRI) have generated interest in functionally segregated connectivity

maps derived from low frequency oscillations of cerebral hemodynamics at rest[68]. This is a simple measure for example in clinical practice. Yet the frequency range analyzed in fMRI connectivity studies is often not in agreement with the typical range reported in non-fMRI literature (see Tables 3, 4 and[69] for discussion). This is of interest because specific bandwidths reflect differential neurophysiologic processes. Further, it is unclear if the spatiotemporal characteristics for these processes are comparable or depict sub processes. It is also unclear which role phase locking or phase shifts might play. Here, for example, in the human low frequency oscillations in sampling volumes of a centimeter have been identified in two bandwidths below 0.1 Hz with a functionally relevant phase-shift[70]. Thus, it is important to re-inspect and further differentiate the spectral information of possible sub-processes of baseline functional connectivity. The perspective being that the simple acquisition of resting state fMRI might offer a novel non-invasive window to further or understanding of neuropathology in the light of autoregulation or baseline cerebral dynamics.

1.4 Previous work of the research group

Previous investigations from our group with Near-Infrared Spectroscopy (NIRS) showed strong cerebral fluctuations of metabolic parameters in two distinct bandwidths (~ 0.04 and ~0.08 Hz)[71]. FMRI has a high spatial resolution and NIRS a high temporal resolution. These two methods offer complementary advantages to investigate mechanisms of cerebral autoregulation in physiological and pathological settings in the brain.

2 Methods and materials

This chapter discusses basic prerequisites for understanding themes pertinent to this dissertation: fundamentals of fMRI and linear and spectral digital signal analysis.

2.1 Fundamentals of Magnetic Resonance Imaging (MRI)

MRI is used to measure proton- and time-dependent changes in brain metabolism with high spatial resolution.

2.1.1 Longitudinal magnetization; the static magnetic field

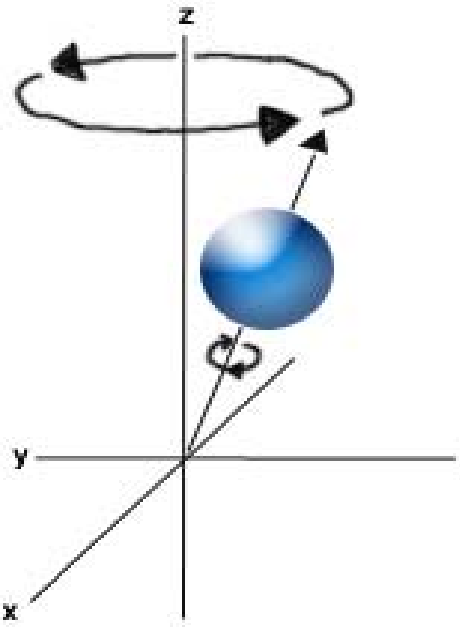

An atom encompasses a shell and a core. The shell consists of electrons. The core consists of protons and neutrons. Protons have a positive electrical charge that spins around the atoms internal axis. This induces a magnetic field. In a B_0 magnetic field of magnetic resonance imaging (MRI) a larger portion of the protons, align parallel versus anti- parallel to the B_0 field. This induces a magnetic vector parallel to the external static magnetic field ("longitudinal magnetization"). This vector precesses with a specific speed around its internal axis ("Larmor frequency"). The precession frequency is directly proportional to the strength of the external magnetic field defined by the Larmor-Equation:

$\omega 0 = \gamma B_0$

ω_0 = precession frequency

γ = gyromagnetic ratio

B_0 = strength of the external Magnetic field in Tesla (T)

2.1.2 Transverse magnetization; the radio wave impulse

The irradiation of a high frequency impulse ("HF- impulse"), frequency locked[1] to the precession frequency, causes transfer of energy and two changes:

- Some protons flip into an anti-parallel alignment, thereby reducing longitudinal and producing transversal magnetization.
- The phase of the protons precession synchronizes. This also contributes to transversal magnetization – the measurable MR-Signal.

The subsequent gyrating decay of longitudinal and transversal magnetization is termed "relaxation".

2.1.3 T1 and T2 relaxation times

Due to resonance effects, the protons lose thermal energy to the surrounding matter ("spin-lattice"). The speed of this process is a function of time described by the time constant T_1 ("longitudinal relaxation time"). Concurrently, the transversal subsystem reverts to its initial state of *null* magnetization ("transversal relaxation") and concurrent proton precession dephases due to minute magnetic inhomogenities in surrounding matter ("spin-spin effects"). This is described as a function of time by the time constant T_2 ("transversal relaxation time"). Relaxation times are tissue specific and the basis for tissue contrast and signal strength.

2.1.4 FMRI; T2* and BOLD

The basis of hemodynamic response to neural functions of the brain was established as long ago as 1890[72]. Many of these metabolic and oxygenation processes can be measured because of their magnetic and paramagnetic characteristics. The most common technique uses the blood oxygen level dependent contrast (BOLD)[33,73-76].

Blood oxygen has, like all substances, characteristic T_1 and T_2 relaxation times. Cortical activation can be identified because deoxyhemoglobin is paramagnetic and oxyhaemoglobin is diamagnetic. In other words, the signal is blood oxygen – or better

[1] Frequency locked HF-impulse: To transfer energy to the protons the frequency of the HF-Impulse has to match, or resonate, with the precession frequency of the protons. This explains the "R" (resonance) in the acronym MRT.

deoxyhemoglobin - level dependent. BOLD fMRI is based on the idea “that neural activation increases regional cerebral blood flow and concomitantly increases venous-blood oxygenation”[77], i.e. decreases ferromagnetic deoxyhemoglobin and precession dephasing. T2 relaxation is based on dephasing that is intrinsic to the molecular environment of the spin (“spin-spin effects”). Chemical shift and local field inhomogenities cause dephasing termed T2’ (prime). The combination of T2 and T2’ yield T2* (star). The rapid dephasing caused by T2* effects is enhanced in areas where there are marked changes in magnetic susceptibility, such as BOLD cortical activity, and is the basis of fast imaging techniques.

2.2 Fundamentals of functional Magnetic Resonance Imaging (fMRI)

Human brain mapping aims to map functional properties to neural correlates of the brain, which results in maps of functional anatomy. Within brain mapping, Neuroimaging defines functional neuroimaging (e.g. with fMRI) with statistical tests for regionally specific effects.

2.2.1 Statistics

Parametric statistics are based on the general linear model that is used in fMRI to make statistical inferences by performing univariate tests at every voxel. This is also known as statistical parametric mapping[78].

The general linear model is derived from analysis of variance. Covariance is the square root of one variable’s variance multiplied by the square root of another variables variance. A more direct indication of how two components co-vary is correlation, i.e. covariance scaled by the product of the respective standard deviations. Linear multiple regression of multiple components is based on partial correlation and defined by the equation:

$y(i) = a + b*x(i) + error$

y = is the dependent variable,

x = independent variable,

b = is the slope, or regression coefficient

a = is the intercept

Thus, linear regression defines the relationship between multiple variables and adds a measure of residual variance as the basis for statistical testing. If the e.g. two variables are related, then when one changes by a certain amount the other changes correspondingly. The parameter b (the regression coefficient) signifies the amount by which change in x must be multiplied to give the corresponding average change in y[2].

The only notable limitations are that multiple linear regression (1) cannot provide a solution for the regression coefficients when the X variables are not linearly independent and (2) the inverse of X'X therefore does not exist. These restrictions, however, can be overcome, and in doing so, the multivariate regression model is transformed into the *general linear model*. The general linear model allows for linear transformations or linear combinations of multiple dependent variables ("y"); e.g., it allows for multivariate testing, multivariate testing of independent linear combination of multiple dependent variables and analysis effects of repeated measure factors with either univariate or multivariate methods.

2.2.2 Statistical Parametric Mapping

Statistical Parametric Mapping (SPM) is a common method for time-domain based analysis of functional connectivity[79]. Generally, the data from each subject is analyzed separately as a series of case studies that are tested subsequently for second level effects. The regions showing e.g. finger-tapping-sensitive responses can be identified in statistical parametric mapping by means of a general linear model. The time-series can be corrected for movement related and/or slice acquisition delay as well as magnetic inhomogenity effects, smoothed in space and time and coregistered or normalized into secondary spaces; e.g. warping of data with 12 degrees of freedom onto an international-standard brain template. Condition-specific effects are assessed by using multiple regression for serially correlated data. Each condition is modeled as a boxcar or stick function and convolved (is there such a word?) with a canonical hemodynamics response function. The statistical model includes global and low frequency confounds. Comparisons amongst conditions are effected with

[2] $y(i) = a + b*x(i) + b_2*x_2(i) \ldots b_n*x_n(i)$

the appropriate contrast of the condition-specific parameter estimates to give statistical parametric maps (SPMs) of regionally specific effects.

2.3 Fundamentals of linear signal analysis

Digital signal processing is the study of signals in a digital representation. In most cases, its goal is to measure or filter continuous real-world analog signals.

2.3.1 Time domain versus frequency domain

Information represented in the time domain describes the “when” and “how much” of an occurrence. Information represented in the frequency domain describes “how often”. For example, a heart rate of 60 beats per minute will peak every second in the time domain and peak exactly once at 1 Hz in the frequency domain. To identify oscillations below 0.1 Hz in a noisy physiological system, the time domain signal is preprocessed and low-pass filtered. The frequency domain offers the advantage that, a peak (i.e. < 0.1 Hz) is identified directly. A common use of Fourier Transform is to find the components of a signal buried in a noisy time domain signal[80].

2.3.2 Time domain analysis

The most straightforward way to implement a digital filter is by convolving the input signal with the digital filter's impulse response. Any signal, x[n], can be decomposed into a group of additive components. Passing these components through a linear system (i.e. convolution) will produce the new signals, y1[n], y2[n] and y3[n]. The synthesis of these output signals is y[n]. To understand how complicated signals are changed by a system, all digital signal processing needs to know is how simple signals (e.g. one single non-zero point) can be shifted and scaled to represent the output of any input. This impulse response is the output of the system when the input is standardized; e.g., the hemodynamic response function is the vascular impulse response of a neural event.

The characteristics, as well as the adverse effects, of every (linear) filter are defined not only by its impulse response, but also by the frequency and step response. These are the Fourier transform and discrete integration of the impulse response, respectively. They are the basis for evaluating a filter's prospective performance. They define the alteration of the frequencies passing through the filter and the strength with which the stop-band frequencies are attenuated. It is important to note that due to e.g. pass-band ripple the processed signal will contain inconsistencies. In contradistinction, the subtraction of one time-domain signal from another will offer a filtered result, which is void, these systematic inconsistencies.

2.3.3 Comparison of filter methods, FIR and IIR

There are two important filter implementation algorithms, FIR and IIR[3]. Both have been used to investigate resting state connectivity. The Butterworth filter was the first and common method[81].. Is one better then the other? A Butterworth filter is a maximally flat (pass-band ripple) Chebyshev. Both the Chebyshev and the windowed-sinc FIR filters are designed to separate one band of frequencies from another. In comparison, both filters generally achieve pass-band flatness and have an ugly step response[4]. Yet, the performance for the windowed-sinc filter is much better than that for the Chebyshev. Thus, "the windowed-sinc is the powerhouse, while the Chebyshev is quick and agile (…). Even if the recursive filter were improved, it is still no match for the FIR performance"[5]. It is like comparing a Ferrari with a go-cart[80].

[3] Finite impulse response (FIR): An impulse response that has a finite number of nonzero values. Often used to indicate that a filter is carried out by using convolution, rather than recursion. Infinite impulse response (IIR)**:** An impulse response that has an infinite number of nonzero values, such as a decaying exponential. Often used to indicate that a filter is carried out by using recursion, rather than convolution.

[4] Which is forgivable for frequency domain filters?

[5] Biswal and colleagues initially used a Butterworth filter and then later suggested that a window-sinc filter is best [82,83].

2.4 Fundamentals of spectral analysis

Spectral analysis allows for the phase independent investigation of and synchronization of phenomena. In other words, “a common use of Fourier Transforms is to find the components of a signal buried in a noisy time domain signal”[80,84].

2.4.1 Major terms defining spectral analysis:

Spectral domain analysis is the frequency-domain representation of a signal as a complex-valued function, characterized by amplitude and a phase function. The representation is computed using a FT (Fourier Transform). The FT can be understood as a degree of correlation of the input signal with cosines and sinus basis functions as a function of frequency. The Power Spectral Density (PSD) is the FT of auto covariance. Thus, the PSD describes the amount of power per unit (= density) of frequency (= spectral) as a function of the frequency. The PSD is calculated in units of power per bandwidth. Power P is defined as the energy per unit of time. If x(k) is the k^{th} value of a time series of N samples with sampling period, its energy E is defined as the sum of the x(k)2 over a predefined time period. Spectral density describes how much signal (energy) is present per unit of bandwidth. The CSD (cross-spectral density) is the FT of cross variance. Coherence has its time domain counterpart in correlation. It is a degree of linear correlation between two signals as a function of the frequency. Coherence and phase are closely connected spectral parameters. Coherence may also be understood as a measure of phase stability that describes the amount of common information of oscillations within certain bandwidths. Two waves are said to be in phase if their crests and troughs meet at the same place at the same time. The waves are out of phase if the crests of one meet the troughs of another. The waves are incoherent if the crests and troughs meet randomly. Thus, correlation is dependent on phase delay. Coherence is dependent on phase stability over time.

2.4.2 Spectral analysis and oscillatory activity

In contradistinction to the time domain, spectral analyses allow us to investigate connectivity of two signals under relative phase shift. This infers connectivity with zero phase-shift, i.e. identical to a correlation analysis, as well as phase stable signals with some amount of phase shift. Thus, spectral analyses should have many possibly

interesting advantages. They are especially equipped to find oscillatory activities and to identify their phase relationship even if these are not phase-locked. In comparison to multivariate spectral methods, the inherently univariate FT-analyses has the drawback of lower resolution and leakage[85]. Yet, in the analysis of oscillatory activity, the disadvantages of transforming the data into the frequency domain should be minor in comparison to time-domain analyses[86].

3 Experimental setup and analysis

The experiment in this study was performed to investigate the bandwidths of resting state connectivity from a set of BOLD-contrast fMRI time-sequences, acquired while the subject *did not* perform any specific task. In order to compare connectivity within well-defined regions of the brain a functional task localized the primary motor cortex prior to resting state investigations.

3.1 Hypothesis

Classically defined low frequency oscillations (0-0.1 Hz) can be subdivided into “very low frequency oscillations” (VLFO, ~0.01-0.5 Hz) and “low frequency oscillations” (LFO, ~0.5-0.1 Hz). We suggest that the motor system will show independent connectivity in both bandwidths. Time domain analyses of functional connectivity have been well investigated, although the LFO and VLFO bandwidth specific analysis is novel. Here in contrast, we argue that frequency domain analyses might be better equipped to identify oscillations in noisy systems.

3.2 Experimental setup

Six subjects (4 male, 2 female, age range 22 through 46 years) performed both experiments. The subjects had no history of neurological or vascular disease, gave

informed consent on participation in the study, which the local Ethics Committee approved, and were financially refunded for their participation.

In experiment 1, the goal was to localize the right and left primary motor cortex (M1). These regions of interest (ROIs) were assessed in the subjects by motor hand stimulation (finger tapping) and the prior knowledge of anatomical landmarks (hand knob of the precentral gyrus).

In experiment 2, the goal was to analyze the functional connectivity of these regions by spontaneous vascular fluctuations, i.e. to demonstrate independent connectivity for the VLFO (Very Low Frequency Oscillations) and LFO (Low Frequency Oscillations) bandwidths.

Each of the subjects underwent the same series of scans performed with 1.5 Tesla Magnetic Resonance Tomograph (Magnetom Vision; Siemens, Erlangen, Germany) equipped with a standard birdcage head coil. The head coil was centered on the nasion. Two way contact between the human test subject and the experimenter was possible due to earphones and a communication system integrated into the MR-scanner. All subjects received a safety ball. Head stabilization with a vacuum pillow as well as the instruction to avoid overt movement for the duration of the experiments attenuated movement artifacts.

High-resolution structural images were acquired using a 1 mm^3 T1-weighted sagittal magnetization prepared – rapid gradient-echo (MPRAGE) sequence (TR: 10 ms; TE: 4 ms; flip angle: 12°; inversion time: 100 ms; 256 x 256 matrix; 170 sagittal slices). Functional images were acquired subsequently with a gradient echoplanar imaging sequence (repetition time (TR): 1000ms, echo time (TE) 60 ms; flip angle: 90°; in-plane resolution: 4x4 mm). Deletion of the first five volumes accounted for T1-saturation effects. Slice orientation was aligned to a diagonal running through the anterior and posterior commissure.

3.2.1 Experiment 1 (“task activation”)

A functional localizer task was used to identify the regions of interest, i.e. the primary motor areas. The subjects executed blocks of 20s unilateral random finger tapping alternating between left and right hand. They received auditory instructions controlled by a stop clock. Resting periods of 40s in duration followed each tapping period (see Figure 4). Thus, 400

volumes of functional magnetic resonance data were acquired, with six axial slices covering the cortical motor areas.

Right (20s.)				Right (20s.)				(…)
	Rest (40s.)		Rest (40s.)		Rest (40s.)		Rest (40s.)	(…)
		Left (20s.)				Left (20s.)		(…)

Figure 4: Localizer task. Finger tapping was evaluated for alternating finger tapping, first RIGHT (Top row) then LEFT (bottom row). Each finger-tapping period lasted 20s. The REST period (middle row) was 40s. Data was acquired over 8 minutes. Each session had six trials (RIGHT – REST – LEFT).

3.2.2 Experiment 2 (“resting state connectivity”);

The six subjects performed no specific task. Both hands were at rest. The subjects were informed to close their eyes, stay awake, and let their thoughts meander (“resting state”). 600 volumes of functional magnetic resonance data were acquired, with six axial slices covering the cortical motor areas.

Rest	Rest	Rest	Rest	Rest	Rest	Rest	Rest	(…)
								(…)
Rest	Rest	Rest	Rest	Rest	Rest	Rest	Rest	(…)

Figure 5: Resting state analysis. In contradistinction to the previous task, both hands were continuously at rest (top and bottom row).

3.3 Analysis

3.3.1 Structural identification of the motor areas (Analysis 1)

The primary motor cortex was identified utilizing the algorithm described by Yousry and colleagues[87]. Although for a number of regions there is a difference between purely anatomical landmarks and the results of functional localization, the primary motor areas can be reliably localized by anatomical landmarks: “the results from fMRI data and surgical validation with intraoperative cortical mapping indicated good correlation of these two methods and that there are no significant differences in the localization of the motor hand area”[88]. This method defines the identification of the primary motor areas, derived from the identification of the omega, or “hand knob” in the axial plane in comparison with the “hand hook” in the sagittal plane in high-resolution structural MRI data. The accuracy of this method is larger than 98%.

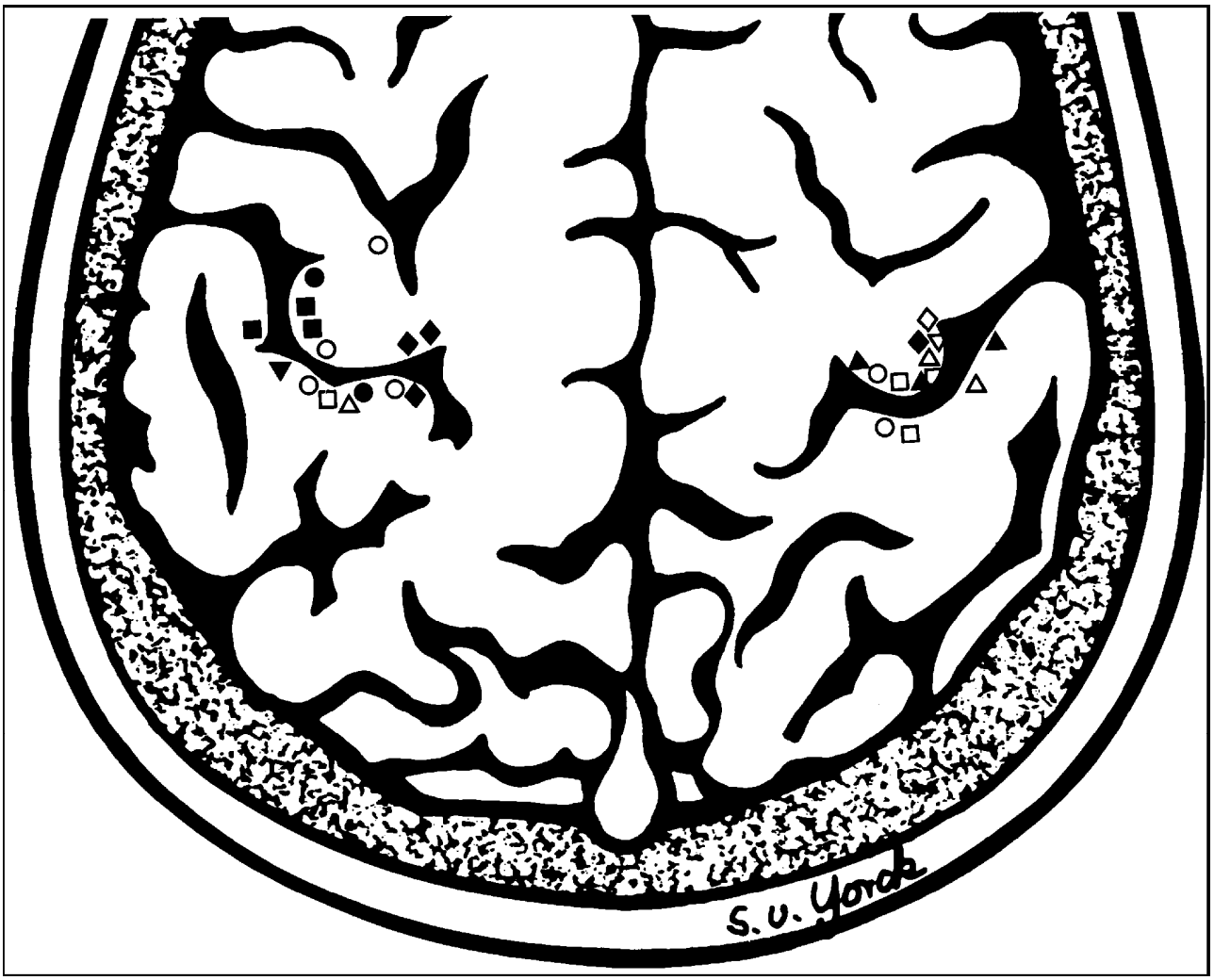

Figure 6: Schematic drawing of the omega shaped motor hand areas collated with maximal activation (intrasulcal activations were discarded) as determined by fMRI in 14 hemispheres from 10 Subjects (see [89]).

3.3.1.1 Functional identification of the motor areas (experiment 1):

Apart from anatomical localization, we performed a motor localizer task. The data from each subject were analyzed separately as a series of case studies. The regions showing finger-tapping-sensitive responses were identified in statistical parametric mapping (SPM, Wellcome Department of Cognitive Neurology, London). The time-series were corrected for movement related effects, smoothed in space (4-mm isotropic Gaussian kernel) and time

(convolution with the canonical hemodynamic response function, Hrf). Condition-specific effects were assessed by using multiple regression analysis for serially correlated data. Each condition was modeled as a box-car function and convolved with the Hemodynamic response function. The statistical model included global and low frequency confounds. Comparisons amongst conditions were effected with the appropriate contrast of the condition-specific parameter estimates to give statistical parametric maps (SPMs) of regionally specific effects correlated with left or right finger tapping.
In all subjects analyzed, the M1-ROI was defined as the region of overlap from the results of the structural and functional analyses.

3.3.2 The analysis of low frequency functional connectivity

The analysis of low frequency functional connectivity is subdivided into two parts: The comparison of VLFO and LFO bandwidths and the comparison of correlation versus coherence as measures of functional connectivity. To investigate these questions it is necessary to define the seed-voxel for a region of interest, e.g. the left M1-ROI. The subsequent analyses measure either the correlation or the coherence of this seed-voxel with all of the other voxel time series in the brain.

3.3.2.1 Extracting resting state VLFO and LFO bandwidths from M1.

The resting state time-series extracted from either M1-ROI were filtered to define five bandwidths. When necessary, digital filter algorithms utilized a forward and backward phase to yield a result with zero phase distortion. The first filter extracted data below 0.015 Hz (VVLFO) as a correlate of machine noise and movement[90], the second below 0.05 Hz, the third above 0.10 Hz. The fourth filter removed high-frequency noise above 0.15 Hz (VHFO) from the analysis that should account for respiratory fluctuations. When possible signals were subtracted from each other to avoid unnecessary artifacts, inherent to digital filters (see methods). Thus, the other frequency bands of interest were extracted in a novel manner as follows:

- The **VLFO** bandwidth was the result of filtering the raw seed-voxel time series with the second filter and subtraction of the VVLFO time-series. The result was a VLFO time-series in the bandwidth from 0.015 through 0.05 Hz.
- The **LFO** bandwidth was acquired by subtracting the results of filter 2 (<0.05 Hz) from the raw time-series, and the results of filter 3 (>0.10 Hz) from this time-series. The result was a LFO time-series in the bandwidth from 0.05 through to 0.10 Hz.
- The **HFO** bandwidth involved subtraction of the result of filter 4 on raw time-series from the result of filter 3 on the raw time-series. Some previous investigations of low frequency functional connectivity included bandwidths below 0.15 Hz.

	Filter 1 *< 0.015 Hz*	Filter 2 *< 0.05 Hz*	Filter 3 *> 0.10 Hz*	Filter 4 *> 0.15 Hz*
VVLFO	*seed* *< 0.015 Hz*			
VLFO		*seed* *0.015-0.05 Hz*		
LFO			*seed* *0.05-0.1 Hz*	
HFO				*seed* *0.1-0.15 Hz*
VHFO				*seed* *> 0.15 Hz*

Table 5: Illustration of seed-voxel filtering algorithm for various bandwidths. The *signals* and their bandwidths are noted in the first *column*. The first row depicts the *filters* and their bandwidths. Signal processing was in accordance to the color scheme: Yellow background indicates row for row the raw signal after first high or lowpass filtering, respective to filters 1-4. The speckled background depicts the bandwidths that were discarded from the initial raw time-series by subtraction. "*Seed*" indicates the bandwidths that were acquired for further analysis. VVLFO: very very low frequency oscillations, VLFO: very low frequency oscillations, LFO: low frequency oscillations, HFO: high frequency oscillations, VHFO: very high frequency oscillations[6].

[6] LFO and VLFO are inline with previous literature. The other abbreviations are only loosely associated and are descriptive in nature. The use of subtraction avoids unnecessary artefacts induced by digital filtering.

	Filter 1 (< 0.015 Hz)	*Filter 2 (< 0.05 Hz)*	*Filter 3 (> 0.10 Hz)*	*Filter 4 (> 0.15 Hz)*
Fpass [Hz]	0.001	0.04	0.09	0.13
Fstop [Hz]	0.015	0.06	0.11	0.15
Astop [dB]	40	40	60	60
Apass [dB]	0.01	0.01	0.01	0.01

Table 6: The four filters utilized in the filtering algorithm: All filters were Window-sinc type filters with a Kaiser window, direct form II Transposed. Fpass: Pass band, Fstop: Stopband, Apass: Passband attenuation, Astop: Stopband attenuation.

3.3.2.2 Low frequency functional connectivity analysis in the time domain

In the resting state, distant areas of the brain that correlated with VLFO and LFO baseline fluctuations of the M1-ROIs were identified. Thus, we were able to generate maps of bandwidth-specific functional connectivity. These bandwidth-specific effects were assessed by using multiple regression analysis for serially correlated data. Thus instead of using a predictor of a functional activation task (see Analysis 1) in the second Analysis we used the filtered time courses of the respective M1-ROI to identify areas, which correlate in their vascular dynamics. In other words, if a pixel showed a similar spontaneous time course as the time course in the M1-ROI this area can be considered 'connective' based on the respective spontaneous vascular oscillation. The statistical model included global as well as high and low frequency confounds. Comparisons amongst conditions were effected with the appropriate contrast of the condition-specific parameter estimates to give statistical parametric maps (SPMs) of regionally and bandwidth specific effects.

At this point, it is essential to understand the meanings of "seed-voxel" and "Hybrid Model". In the previous passage, the descriptive term "reference area" and "low-frequency fluctuations" (from the reference area M1-ROI) were used descriptively. The term seed-voxel is misleading. It is commonly understood to depict the first principle component or mean from a certain number of time-series extracted from a region of interest. Importantly,

one can state, that these time-series represent the best estimate of the vascular signal in a specific region. This is in contradistinction to a boxcar model of hypothesized neural activity derived from the experimental task that is then transformed into a vascular model by means of convolution with a hemodynamic response model. The term “Hybrid Model” denotes a vascular signal (e.g. the “seed-voxel”) extracted from a specific region (e.g. M1-ROI), which is regressed on a voxel by voxel basis against the functional images it was extracted from.

The VLFO or LFO seed-voxels were contrasted against a complex baseline. This included the VVLFO, HFO and VHFO bandwidths, or low frequency noise, respiratory and higher frequency noise, respectively. Further, both the general mean time course and the realignment parameters were entered as covariates of no interest. Please see Figure 7. Prior to analysis, the data had been corrected for movement related effects and smoothed in space (6-mm isotropic Gaussian kernel).

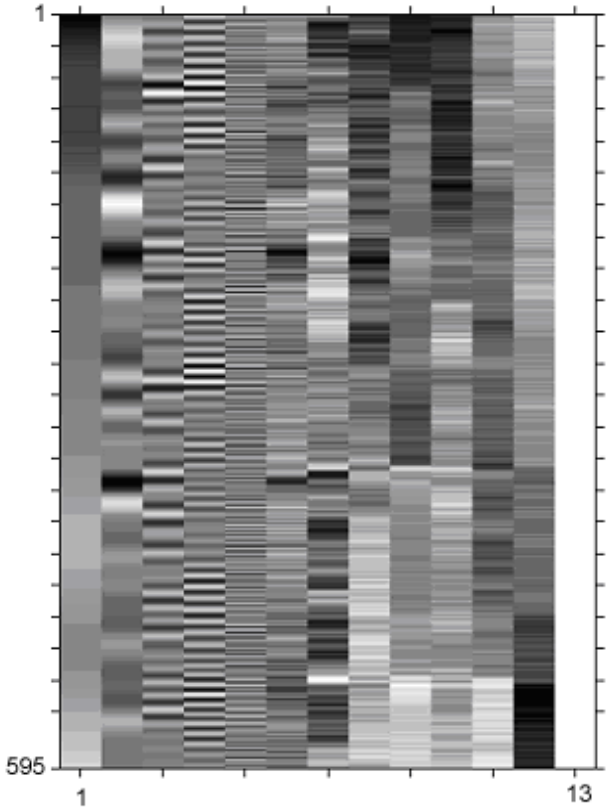

Figure 7: Design matrix of fMRI analysis.
Ordinate: fMRI volume number.
Abscissa: 1: VVLFO, 2: VLFO, 3: LFO,
4: HFO, 5: VHFO,
6: general mean timecourse,
7-12 realignment parameters
(x-translation, y-translation, z-translation,
x-roll, y-roll, z-roll)
13: constant

A fixed effects second level analysis was applied to the results from the single subject case studies to identify the average functional connectivity. This was effected within the SPM framework, a multisubject design in normalized data space and for the left and right M1-ROI individually.

3.3.2.3 Low frequency functional connectivity analysis in the spectral domain:

In contradistinction to time domain analyses, spectral analysis allows one to avoid filtering and to estimate the coherence as well as the phase-shift between time-series and is better suited to identify oscillations in noisy time-series. In analogy to the temporal analysis, the data from each subject were analyzed separately as a series of case studies. Regions showing low-frequency fluctuations coherent (phase stabile) with the reference seed-voxel were identified. The reference time-series were corrected for movement related effects and smoothed in space (4-mm isotropic Gaussian kernel). The voxel by voxel analysis of coherence was implemented in the MATLAB 6.5 environment. The estimation used the Welch's averaged periodogram method, to estimate values of coherence, as a function of frequency, with values between 0 and 1 that indicate how well a given voxel time-series (595 samples) is coherent with the "seed-voxel" time-series (595 samples). Prior to analysis the seed-voxel was divided into overlapping (127+1 samples) hanning windows (256 samples) and zero padded to the length of NFFT (1024). The voxel by voxel whole brain coherence analysis gave spatial maps of coherence for frequencies. The VLFO were encoded in the first 26 maps, LFO in the following 26 maps. The first map in VLFO was discarded to account for noise[91]. Thus, the spatial map of VLFO coherence was defined as the grand average of the first 26 maps and LFO by the average of the following 26 maps. An example of the coherence across the different frequencies is given in Figure 8.

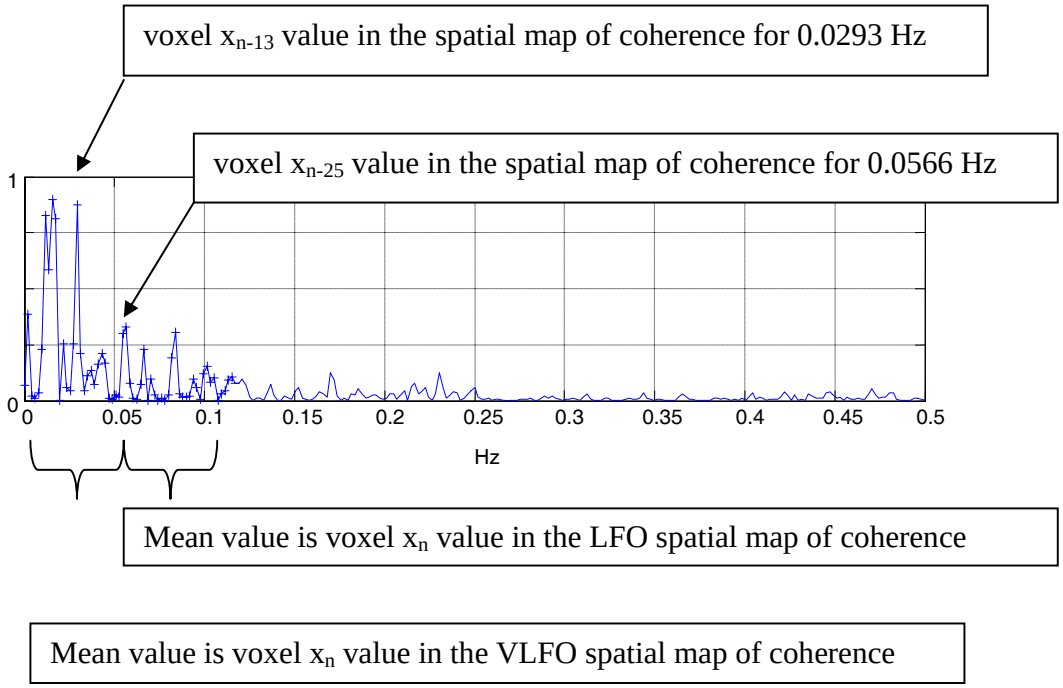

Figure 8: Exemplary plot of coherence between the seed-voxel and a voxel in the contralateral primary motor cortex. The ordinate depicts coherence. The abscissa depicts the bandwidth. This plot gives one value at the position *n* for a spatial map of coherence at a given bandwidth (e.g. 0.0293 or 0.0566 Hz). The average value over multiple bandwidths give the value for either VLFO or LFO spatial maps of coherence at position *n*, e.g. in this case a contralateral M1 time-series. This method is considered to be stable across subjects with slight variations in their peak frequency power with in the respective bandwidth.

The spatial maps of coherence for VLFO and LFO were thresholded for significance[92]. Essentially the degrees of freedom are given by the number of samples per window (595/256 + windows due to overlapping) plus ½ times a factor derived from the window type (Hanning = 2.5). The degrees of freedom can be plotted as a function of coherence. The threshold for e.g. $p<0.05$ can be read from this graph – in this case 0.73.

For the second level analysis, all coherence maps were transformed into a normalized space. To this effect, the individual T1-images were warped with 12 degrees of freedom to best fit a standardized template[93]. Then the individual coherence maps were coregistered to that subjects structural T1-image and the T1-transformation parameters were subsequently applied to the coregistered coherence maps. This transformation algorithm was applied *after* statistical inference.

Within standardized space, the spatial maps of coherence, across all subjects, can be calculated for any given frequency. For example, six subjects' coherence maps at the frequency of 0.34 Hz could be summed together and divided by 6. This approach would be with flaw because coherence is defined as CSD /PSD*PSD. We corrected for this interdependency between nominator and denominator, calculated the mean CSD over all subjects, and divided it by the product of the two mean PSDs over all subjects.

4 Results

In the first experiment**,** "identification of the motor areas"**,** the goal was to identify the bilateral homologous primary motor cortices defined by structural landmarks (experiment 1, part 1) as well as by sequential finger tapping (experiment 1, part 2). In the second Analysis "interactions of baseline fluctuations", the goal was to investigate the connectivity of these areas in non-activated data sets with both temporal and spectral domain analyses. Our hypotheses were that connectivity would be found in both the VLFO and LFO bandwidths, with both temporal and spectral analyses.

4.1.1 Structural identification of the motor areas

The identification of structural landmarks of the primary hand motor successfully utilized the algorithm suggested by Yousry and colleagues[94], described in detail in the methods chapter. These anatomical results (M1-ROIstruct) defined the *structural constraints* for the identification of the M1 Region of Interest (M1-ROI).

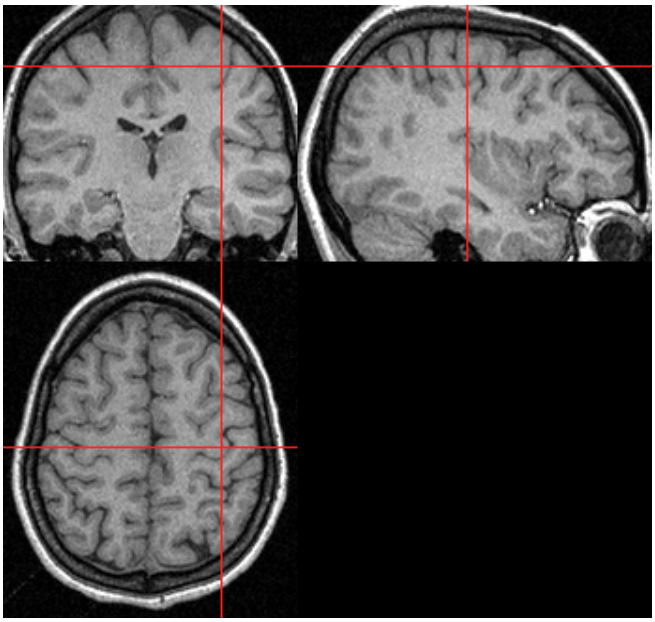

Figure 9: This figure depicts the “hand-knob” in an exemplary subject as identified by the method described by Yousry and colleagues[95]. The cross hair indicates the hand knob. Image 1 shows the hand knob in the coronal, sagittal and axial orientation in T1-weighted MRI. Image 2 shows the zooms of the left and right hand knobs, relative to relevance in the identification algorithm, i.e. in axial, sagittal and coronal projections, from top down. Image 2 will be the structural background for the functional results in the following chapters.

4.1.2 Functional identification of the motor areas

The motor areas were identified with the localizer algorithm from experiment one. As expected, both of the bilateral motor areas were easily identifiable for all single subjects. In general conservative thresholds were used (p corrected <0.05, cluster > 10 voxels) throughout this stage of analysis to facilitate the identification of a circumscribed and highly specific clusters. These results (M1-ROIfunct) defined the *functional constraints* for the identification of the M1-ROI.

Thus, the M1-ROI was confined by the overlap of M1-ROItask and M1-ROIstruct. Exemplary results from one subject are rendered onto the extracted brain surface in Figure 10 and quantified in Tabel 4.

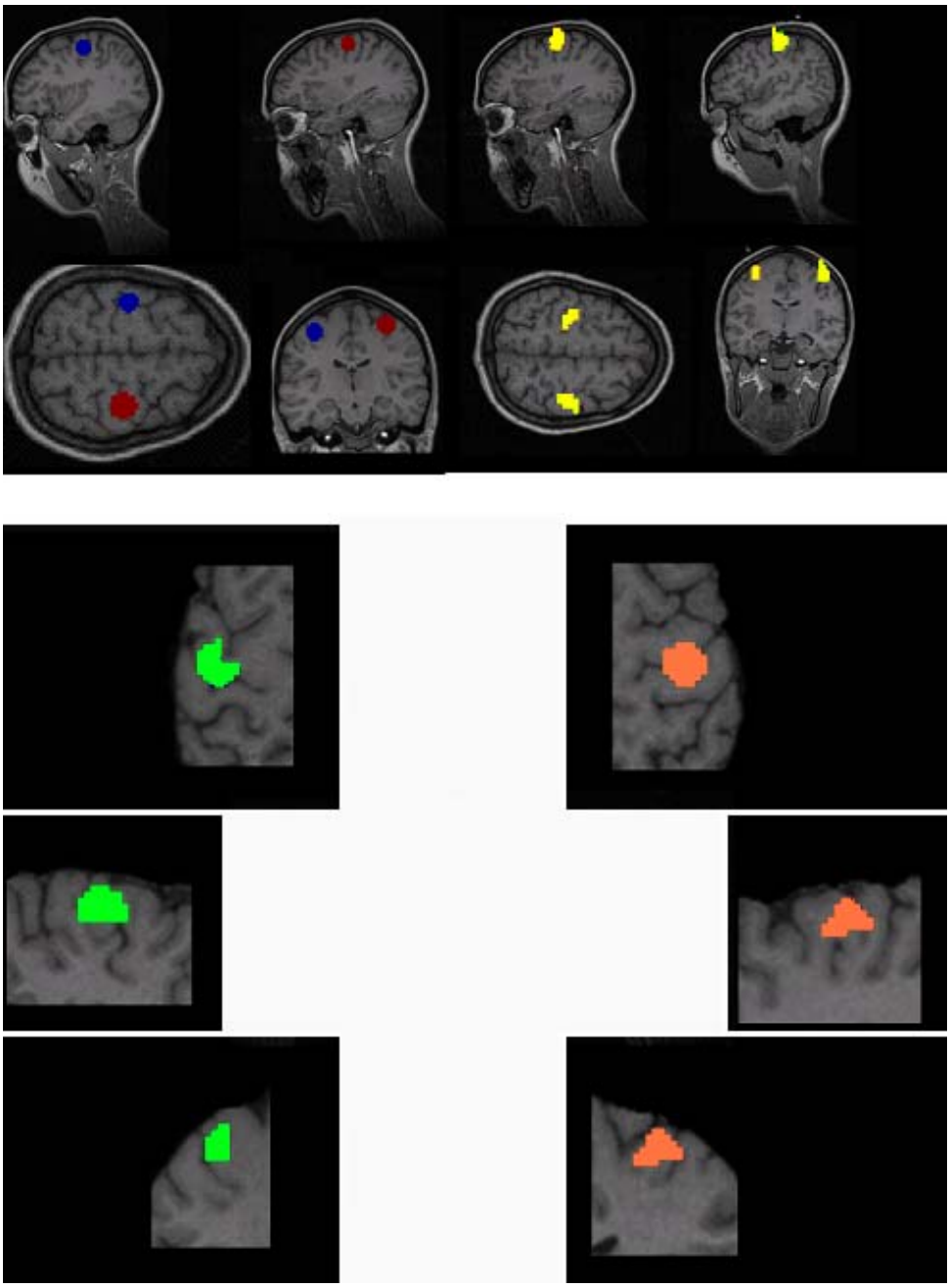

Structural localization (M1-ROIstruct)			***Finger tapping (M1-ROIfunct)***		***Overlap (M1 ROI)***	
	mm^3	COM	mm^3	COM	mm^3	% overlap
Left:	2168	-42 -3 +63	2563	-42 -6 +70	1360	62,73%
Right:	2160	+19 -6 +69	2322	+21 -8 +72	1192	55,19%

Figure 10: Image 1: The identification of the M1-ROI: structural localization (red and blue) and finger-tapping (yellow) in sagittal, axial and coronal orientation. Image 2: Zooms portray their overlap for left (blue & yellow = green) and right (red & yellow = orange).

Table 7: Overlap of the structural ROI and the functional ROI, for left as well as right hemisphere. The volume of the ROIs are given in cubic mm. COM is the center of matter of the ROIs in mm. The percent overlap, is the percent overlap of structural ROI /overlap ROI.

4.2 Functional connectivity of the motor areas

The aim is to quantify the VLFO and LFO connectivity in the temporal and spectral domains.

4.2.1 Temporal connectivity

The overlap between the contralateral M1-cluster (M1-ROIcorr) and the respective M1-ROI offer a measure of the functional connectivity between the bilateral M1-ROI's[96]. Conservative thresholds (p corrected <0.05, cluster > 10 voxels) facilitated the identification of circumscribed and highly specific clusters in the bilateral primary motor cortices. The contralateral overlap was on average 44.71% (VLFO) and 28.24% (LFO) for the left hemisphere (right hemispheric seed-voxel) and 56.38% (VLFO) and 21.76% (LFO) for the right hemisphere (left hemispheric seed-voxel), respectively (see Tables 8 and 9). The mean ipsilateral overlap was always larger than 90%. This high ipsilateral connectivity is due at least in part to the fact that the predictor is being correlated with the M1-ROI time courses it was extracted from (Hybrid-model, see Methods chapter).

For all subjects the volume of the M1-ROI (average 7040 +/- 3003 mm^3) defined by conjunction of finger-tapping induced activity and anatomical landmarks was always larger then the M1-ROIcorr (average 6486 +/- 3006 mm^3). These two ROIs never overlapped completely (average 39.02% +/- 18.14%).

There was no significant difference between the bandwidths. All subjects supplied evidence for contralateral connectivity to the contralateral primary motor area and in some cases the supplementary motor area (SMA).

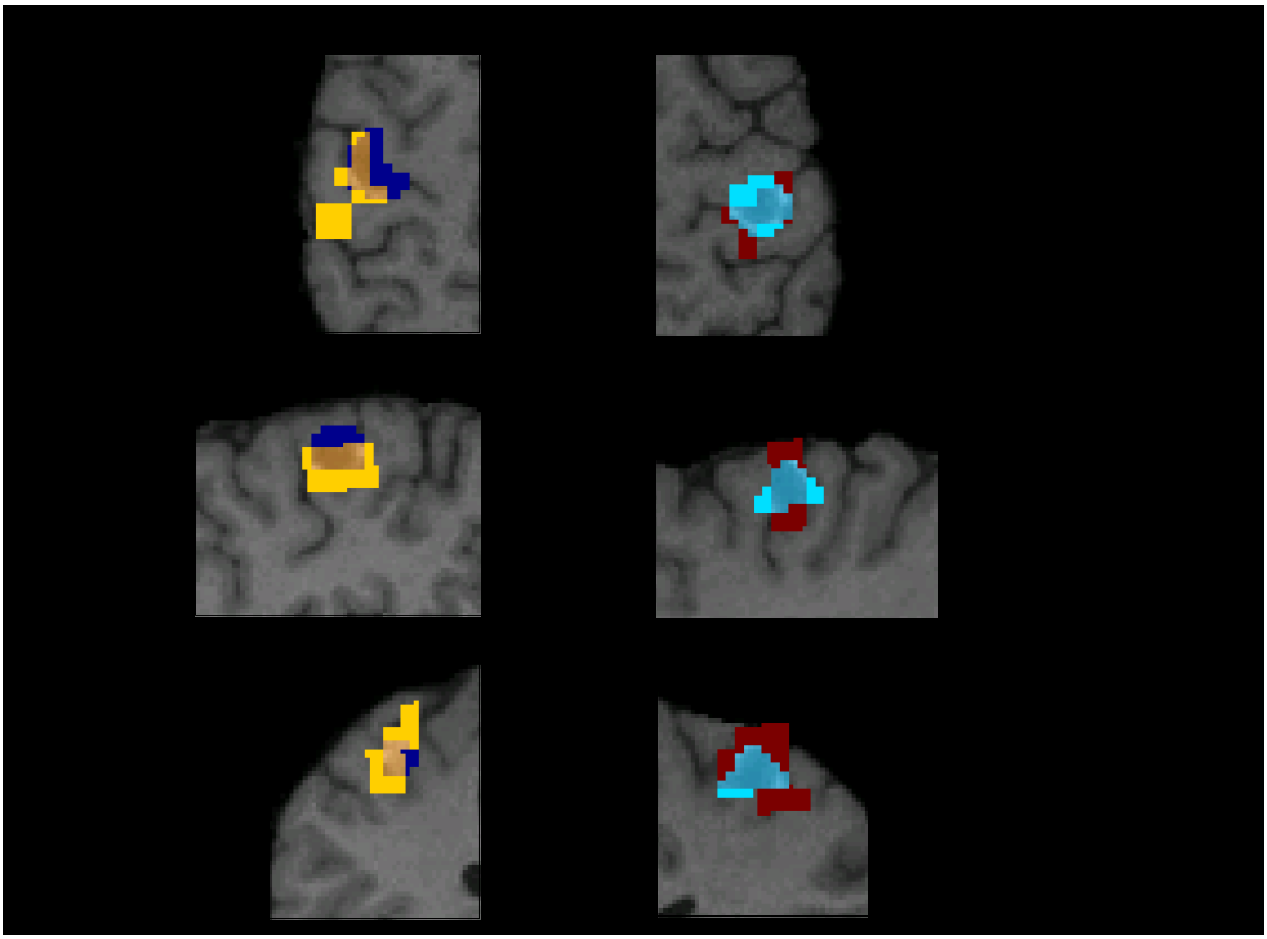

VLFO correlation (single subject)			*Overlap with finger tapping ROI*		*Overlap with M1 ROIs*	
	mm^3	stats	mm^3		mm^3	
Left:-ROI	4244	p < 0.05	1952	*45,99%*	608	*44.71%*
Right-ROI	2082	p < 0.05	1344	*64.55%*	672	*56.38%*

Figure 12: VLFO connectivity. Overlap of M1-ROIvlfo (yellow or red) with the M1-ROIs (blue or cyan) for an exemplary subject. Left is left and right is right. The results for ipsilateral connectivity are not displayed. The first row is the axial, the second the sagittal and the third the coronal plane. The background image is a T_1-MRI from the same subject shown in figure 11.

Table 8: Overlap Ratio of M1-ROIvlfo and M1 ROIs. Overlap of the motor regions connected by correlated spontaneous vascular fluctuations of left and right M1-ROI. The volumes of the ROIs are given in cubic mm. The stats are the p-values, bonferonni and threshold corrected. The percent overlap, is the percent overlap of the M1-ROIvlfo mm^3 *per* M1-ROI mm^3.

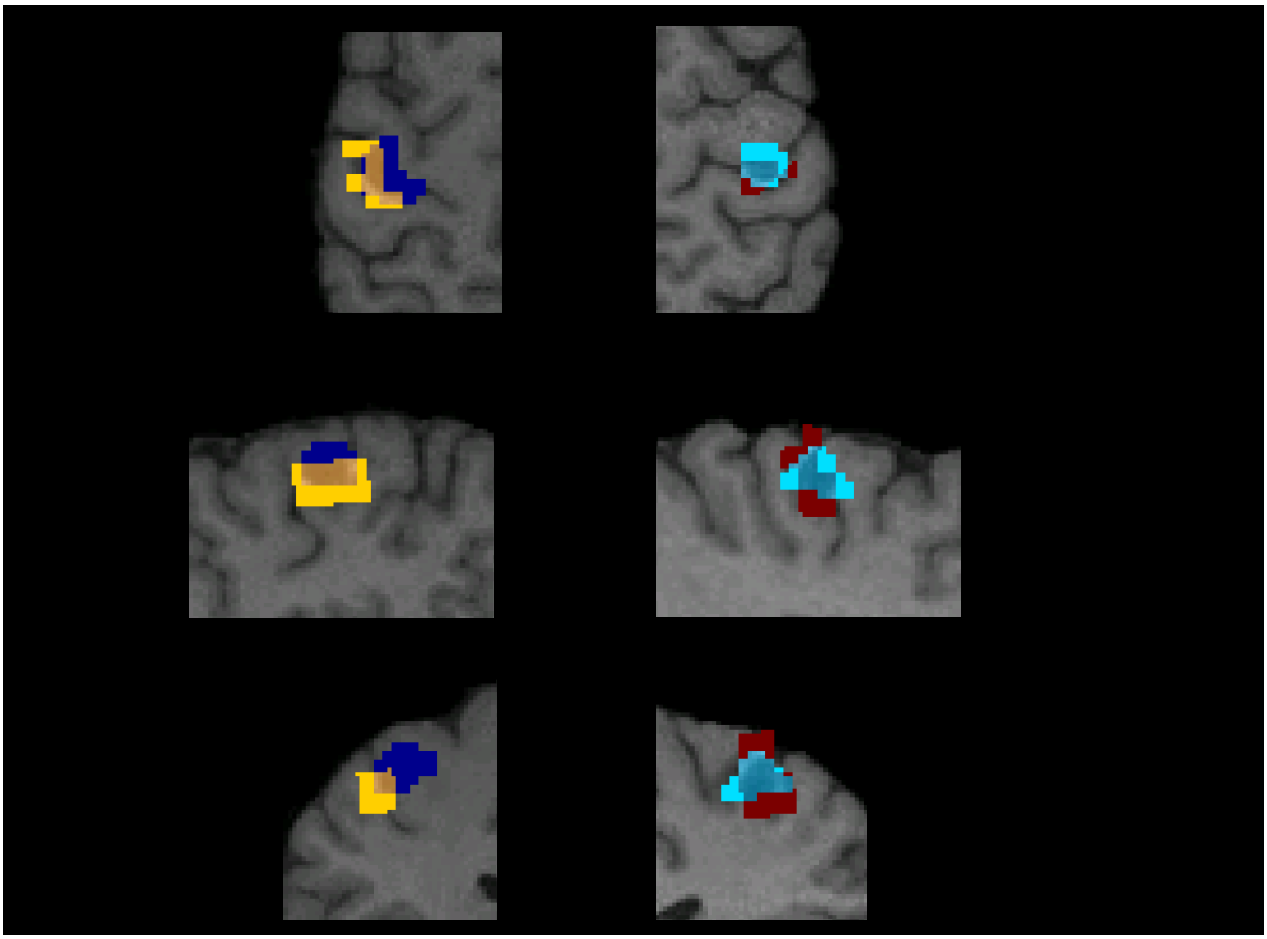

LFO correlation (single subject)			*Overlap with finger tapping ROI*		*Overlap with M1 ROIs*	
	mm^3	stats	mm^3		mm^3	
Left:	1922	p < 0.05	552	*21,54%*	384	*28.24%*
Right:	1201	p < 0.05	400	*15.61%*	296	*21.76%*

Figure 13: M1-ROIlfo connectivity. Overlap of M1-ROIlfo connected regions (yellow or red) with the M1-ROIs (blue or cyan) for an exemplary subject. Left is left and right is right. Results for ipsilateral connectivity are not displayed. The first row is the axial, the second the sagittal and the third the coronal plane.

Table 9: Overlap Ratio of M1-ROIlfo and M1-ROIs. Overlap of the motor regions connected by correlated spontaneous vascular fluctuations of left and right M1-ROIs. The volumes of the ROIs are given in cubic mm. The stats are p-values, bonferonni and threshold corrected. The percent overlap, is the percent overlap of the M1-ROIlfo mm^3 *per* M1-ROI mm^3.

4.2.2 Spectral connectivity

The overlap between the contralateral coherence-connectivity M1-cluster (M1-ROIcoh) and the respective M1-ROI offer a measure of the coherence-based connectivity between the primary motor cortices. The contralateral-from-seedvoxel overlap was on average 62.35% (VLFO) and 25.29% (LFO) for the left hemisphere (right sided seed-voxel) and 55.70% (VLFO) and 71,14% (LFO) for the right hemisphere (left sided seed-voxel) for VLFO and LFO functional connectivity, respectively. Conservative thresholds ($p < 0.05$, cluster >10 voxels) facilitated the identification of circumscribed and highly specific clusters. The ipsilateral overlap was always larger than 90%.

For all subjects the contralateral M1-ROI (average 7040 +/- 3003 mm^3) was always larger than the M1-ROIcoh (average 5293, 54 +/- 3172, 59 mm^3). These two ROIs never overlapped completely (average 36.83% +/- 20.19%).

In spectral analysis, the bilateral M1-ROI spontaneous fluctuations were highly coherent in both the VLFO and LFO bandwidths. All subjects supplied evidence for contralateral coherence-based connectivity of the primary motor area and in some cases in the SMA in both bandwidths. High ipsilateral coherent connectivity is at least in part due to the Hybrid-model algorithm (see methods chapter).

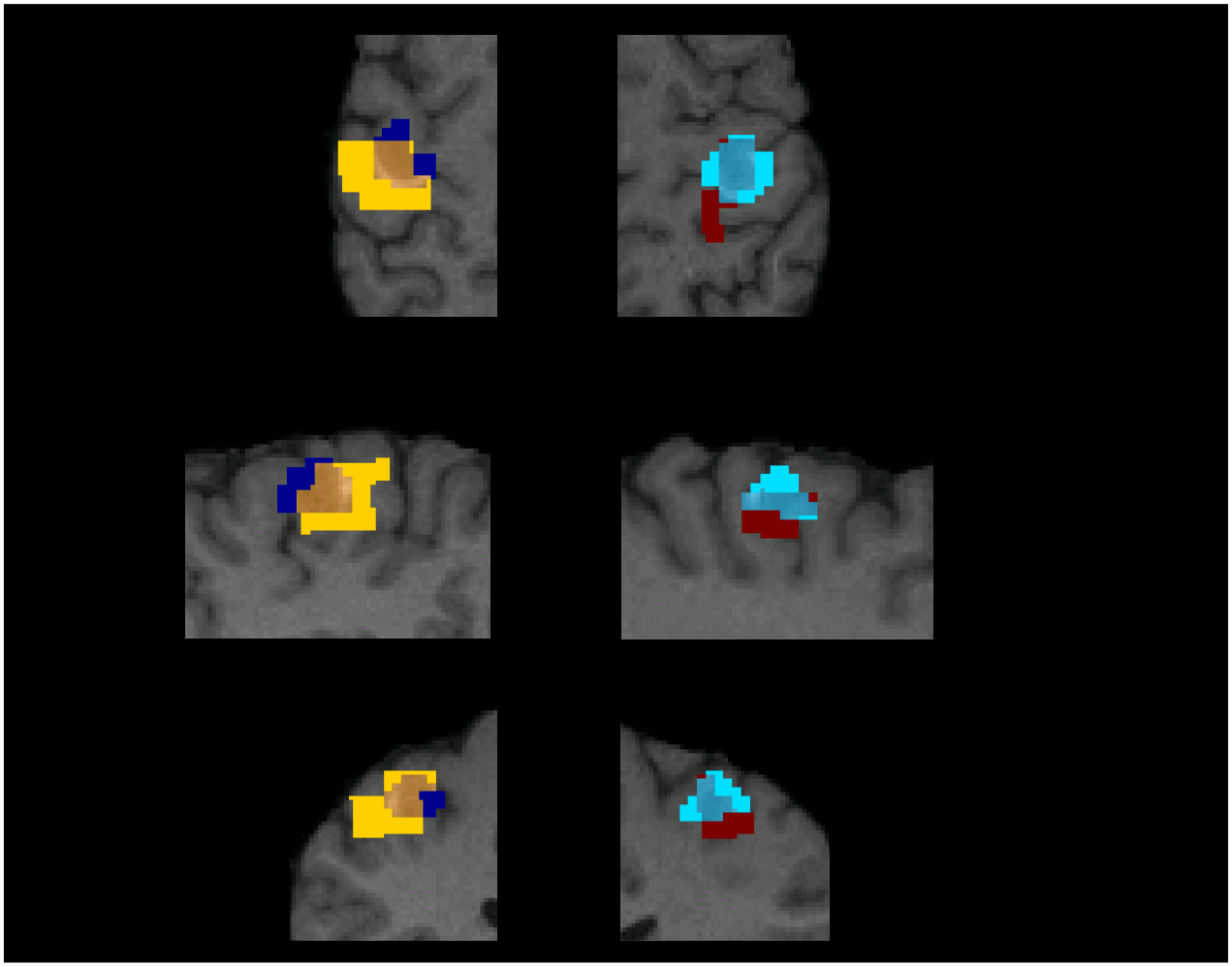

VLFO coherence (single subject)			*Overlap with finger tapping ROI*		*Overlap with M1 ROIs*	
	mm^3	stats	mm^3		mm^3	
Left:	3923	$p < 0.05$	2040	*52,00%*	848	*62,35%*
Right:	1762	$p < 0.05$	664	*37,68%*	664	*55,70%*

Figure 14: Bilateral M1-ROI VLFO-Coherence. The zooms portray the overlap of VLFO coherently connected regions (yellow or red) with the structure-task ROIs (blue or cyan) for an exemplary subject. Left is left and right is right. The first row is the axial, the second the sagittal and the third the coronal plane.

Table 10: Overlap Ratio of VLFO-coherence and M1-ROIs. Overlap of the motor regions with coherent spontaneous vascular fluctuations of left and right M1-ROIs. The volumes of the ROIs are given in cubic mm. The percent overlap, is the percent overlap of the VLFO-ROI mm^3 *per* M1-ROI mm^3.

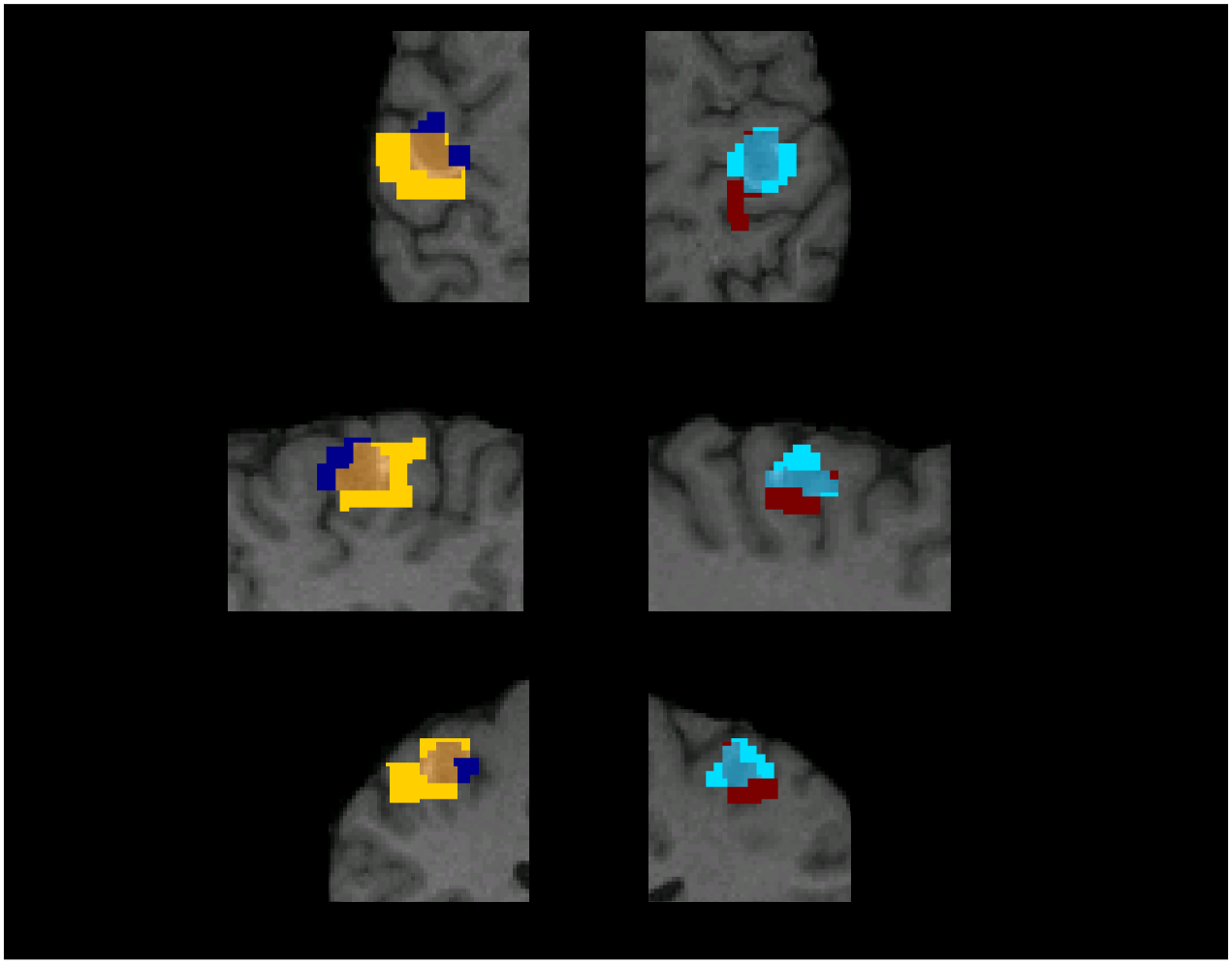

LFO coherence (single subject)			*Overlap with finger tapping ROI*		*Overlap with M1 ROIs*	
	mm^3	stats	mm^3		mm^3	
Left:	1361	$p < 0.05$	592	*43,50%*	344	*25,29%*
Right:	2723	$p < 0.05$	1360	*49,94%*	848	*71,14%*

Figure 15: Bilateral M1-ROI LFO-Coherence. The zooms portray the overlap of LFO coherently connected regions (yellow or red) with the structure-task ROIs (blue or cyan) for an exemplary subject. Left is left and right is right. The first row is the axial, the second the sagittal and the third the coronal plane.

Table 11: Overlap Ratio of LFO-coherence and M1 ROIs. Overlap of the motor regions with coherent spontaneous vascular fluctuations of left and right M1-ROIs. The volumes of the ROIs are given in cubic mm. The percent overlap, is the percent overlap of the LFO-ROI mm^3 *per* M1-ROI mm^3.

5 Group results

The single subject analysis offered evidence that the connection between the bilateral motor cortices can be visualized by analysis of both VLFO and LFO bandwidths. This could be observed in both temporal and spectral analyses. The aim of the group analysis was to investigate statistical tests on our hypotheses that connectivity will be found in both the VLFO and LFO bandwidths, with both temporal and spectral analyses. We find independent connectivity in both bandwidths. Further, we find that spectral analyses might be better equipped to depict low frequency connectivity and that there is no significant difference of connectivity strength for the LFO and VLFO bandwidths.

5.1 Connectivity in the VLFO and LFO bandwidths

The connectivity maps between the primary motor cortices for both VLFO and LFO bandwidths were confirmed in the group analysis. Interestingly strong connectivity to the SMA could also be found on the group level for both bandwidths and both analyses. Further, distant activations in the primary sensory cortices are clearly discernable on the postcentral sulcus (see Figure 16).

Figure 16: Surface projections of the results from the VLFO and LFO correlation connectivity analysis. The first row displays maps of areas connected to the left (L) M1, the second row areas connected to the right (R) M1-ROI. The activations are overlaid semitransparent to accommodate recognition sulcal and gyral anatomy. Connectivity is seen in the primary and secondary sensorimotor areas bilaterally (i.e. M1, S1 and SMA) for both left and right seed-voxels as well as for VLFO and LFO bandwidths.

Figure 17: Surface projections of the results from the VLFO and LFO coherence connectivity analysis. The first row displays maps of areas connected to the left (L) M1, the second row areas connected to the right (R) M1-ROI. The activations are overlaid semitransparent to accommodate recognition of sulcal and gyral anatomy. Connectivity is seen in the primary and secondary sensorimotor areas bilaterally (i.e. M1, S1 and the

mesial parietal wall, e.g. SMA) for both left and right seed-voxels as well as for VLFO and LFO bandwidths.

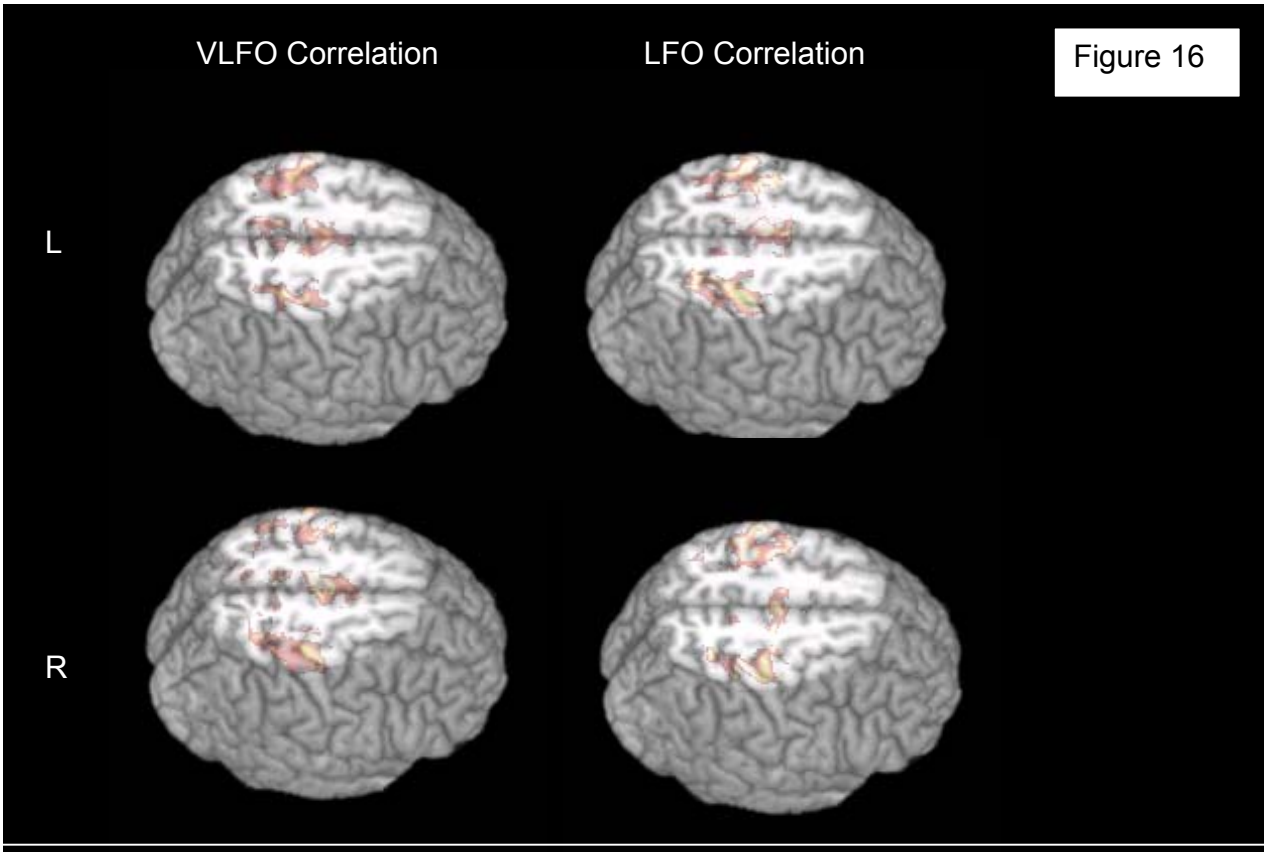

Figure 16

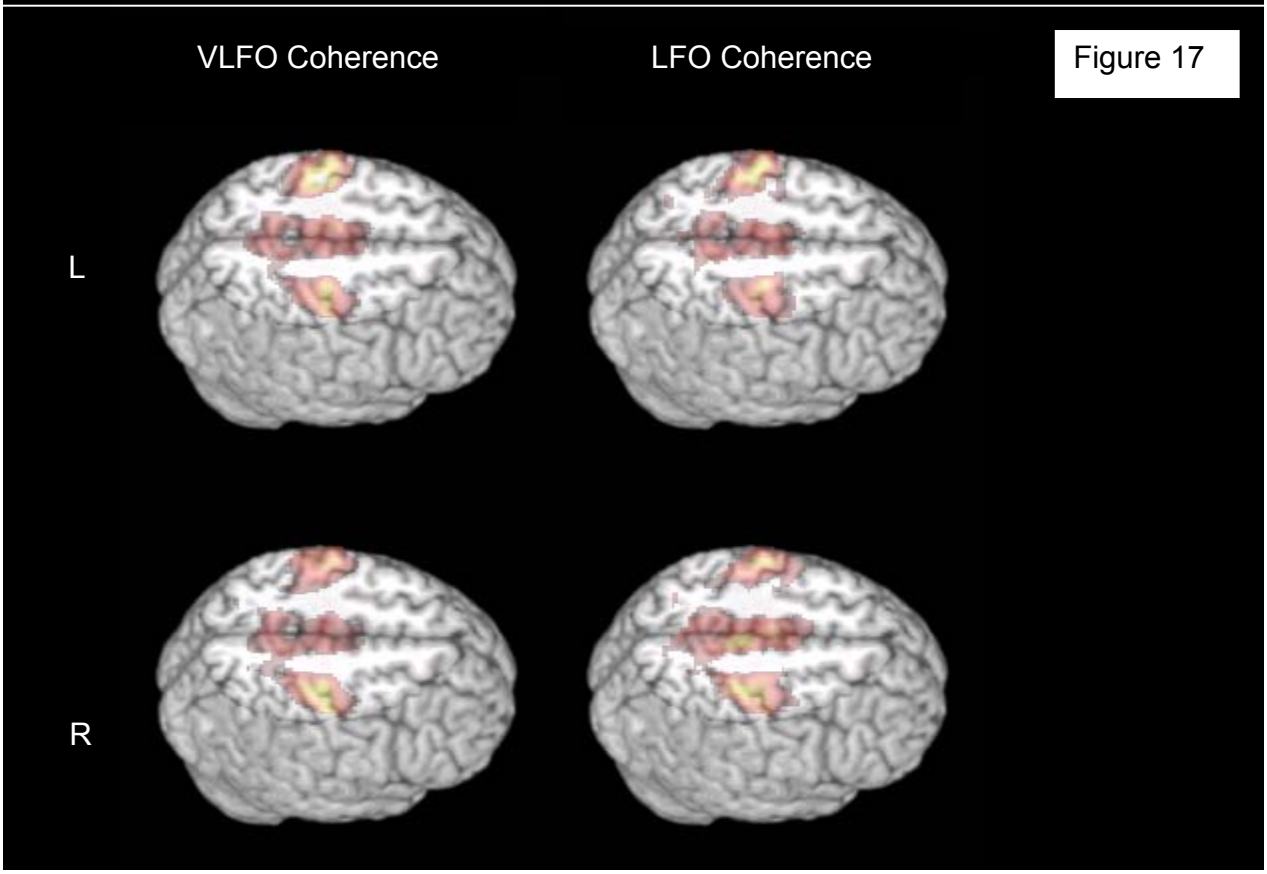

Figure 17

	Correlation/ Coherence (CC)	Finger-Tapping (FT)	Structural (S)	M1-ROI (FT&S)	*CC & FT*	*CC & M1-ROI*
	mm^3	mm^3	mm^3	mm^3	mm^3	mm^3
VLFO correlation (group)						
Left:	8208 $^{+}$/- 2974	6808 +/- 3667	*2099 +/- 199*	*1085 +/- 257*	2686^{+}/*-1448*	539^{+}/*-185*
Right:	6006 $^{+}$/- 3052	7608 +/- 2232	*2120 +/- 141*	*1069 +/- 312*	2225^{+}/*-1231*	439^{+}/*-365*
LFO correlation (group)						
Left:	5618 $^{+}$/- 3600	6808 +/- 3667	*2099 +/- 199*	*1085 +/- 257*	1987^{+}/*-1201*	439^{+}/*-392*
Right:	6111 $^{+}$/- 2352	7608 +/- 2232	*2120 +/- 141*	*1069 +/- 312*	2227^{+}/*-1156*	480^{+}/*-415*
VLFO coherence (group)						
Left:	5884 $^{+}$/- 2822	6808 +/- 3667	*2099 +/- 199*	*1085 +/- 257*	2308^{+}/*-1077*	461^{+}/*-282*
Right:	6056 $^{+}$/- 4877	7608 +/- 2232	*2120 +/- 141*	*1069 +/- 312*	1380^{+}/*-1085*	476^{+}/*-392*
LFO coherence (group)						
Left:	4617 $^{+}$/- 2443	6808 +/- 3667	*2099 +/- 199*	*1085 +/- 257*	1643^{+}/*-1231*	400^{+}/*-355*
Right:	4617 $^{+}$/- 2523	7608 +/- 2232	*2120 +/- 141*	*1069 +/- 312*	1388^{+}/*-766*	420^{+}/*-409*

Table 12: M1-ROI Correlation and Coherence connectivity with respect to bandwidth. Overlap of the motor regions with correlated or coherent spontaneous vascular fluctuations of left and right M1-ROIs. This is defined as the measure of connectivity. The ROI volumes are given in cubic mm. The percent overlap, is the percent overlap of the VLFO-ROI mm^3 *per* M1-ROI mm^3.

5.1.1 VLFO versus LFO connectivity

Two-sided paired T-test tested for significant differences in VLFO versus LFO and coherence versus correlation. No significant differences were found. Also, in factorial testing no significant interactions were found for any of the subgroups.

Table 13: Paired t-Test on VLFO versus LFO results.

	Variable 1	*Variable 2*
Mean	0,4417608	0,36522563
Variance	0,05672065	0,09375485
Observations	24	24
Pearson correlation	0,40013315	
Degrees of freedom(df)	23	
t-Statistic	1,23536738	
P(T<=t) one-sided	0,11458221	
Critical t-value for one-sided t-Test	1,71387152	
P(T<=t) two-sided	0,22916442	
Critical t-value for two-sided t-Test	2,0686576	

5.1.2 Coherence vs. correlation

Two-sided paired T-test tested for possible differences in coherence versus correlation. No significant factorial interactions were found in any of the sub-analyses.

Table 14: Paired t-Test on Correlation versus Coherence analysis results

	Variable 1	*Variable 2*
Mean	0,42418922	0,38279721
Variance	0,07414601	0,07849175
Observations	24	24
Pearson correlation	0,78052444	
Degrees of freedom(df)	23	
t-Statistic	1,10709599	
P(T<=t) one-sided	0,13984857	
Critical t-value for one-sided t-Test	1,71387152	
P(T<=t) two-sided	0,27969713	
Critical t-value for two-sided t-Test	2,0686576	

5.2 Summary

Two analyses were performed on six subjects (4 male, 2 female, and age range 22 through 46). We found that (i) the functional localizer task easily identified the functional anatomy that coincided well with the structural landmarks described by Yousry and colleagues, (ii) that functional connectivity was found in both the LFO and VLFO bandwidths by coherence as well as by correlation analysis, (iii) no approach proved to be superior. Further results suggested distant connectivity with sensory and secondary motor areas. The box plot of the data might suggest a trend towards a more efficient analysis in the VLFO bandwidth with spectral analyses (Figure 18), which will be discussed in the next chapter.

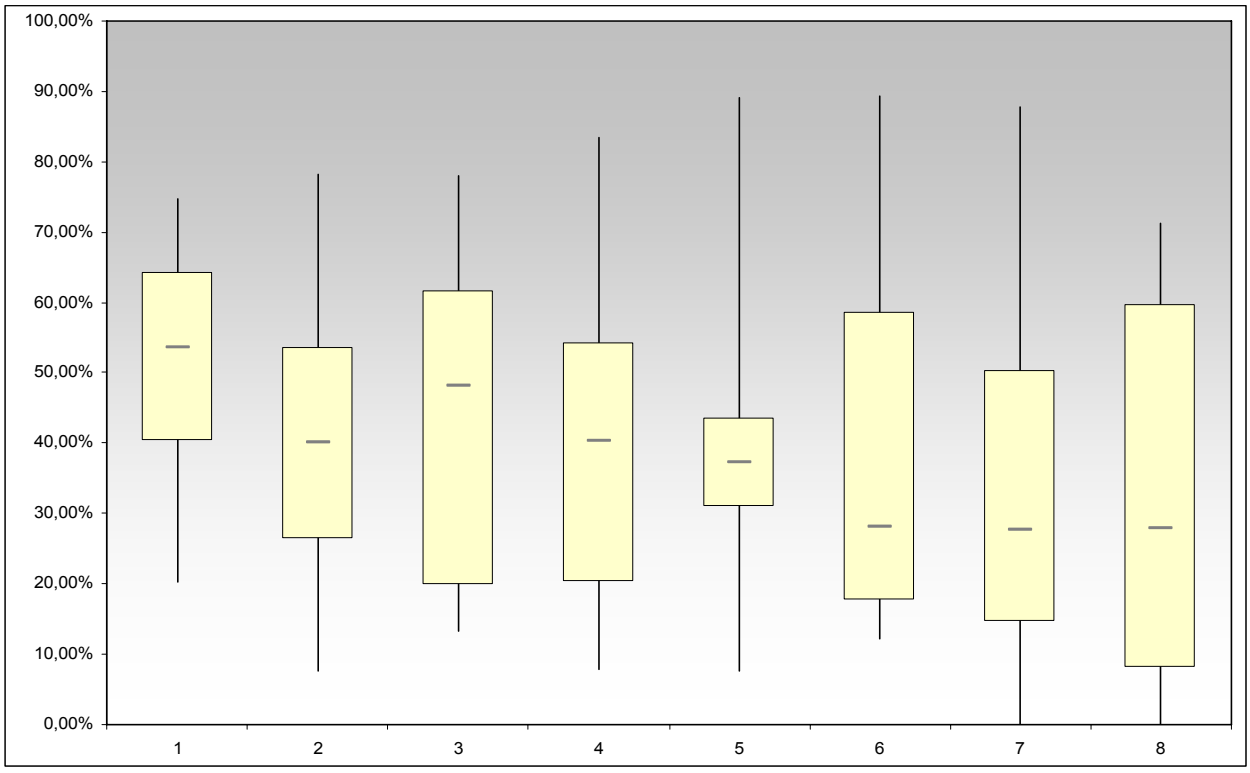

Figure 18: Box plot chart synopsis of group results of correlation versus coherence analysis and VLFO versus LFO analysis. The highest value is the maximum, the lower most the minimum value. The upper border of the box is the upper quartile (75%) and the lower border the lower quartile (25%). The midline mark is the median. All values are in percentage of overlap of the coherence or correlation ROI with the M1-ROI identified with structural and functional measures.

6 Discussion

As described in the results section, with two simple and straightforward approaches, we found connectivity of low and very low frequency fluctuations of the BOLD signal change in fMRI of the human brain. These results confirm previous invasive and non-invasive studies - in animal and man - of low frequency fluctuations of hemodynamics. Initially seen as a derivative of vasomotion or autoregulation, recent evidence in fMRI suggests a neurovascular coupling due to spatial maps of functional relevance. We found that two bandwidths of low frequency functional connectivity can be differentiated, argue that spectral analyses might best situated to study functional connectivity and discuss how low frequency oscillations might confound fMRI studies.

6.1 LFO and VLFO

Low frequency oscillations of cerebral circulation have been defined below 0.1 Hz, but can be further differentiated in “low frequency” bandwidth (0.05-0.1 Hz, LFO) and a “very low frequency” bandwidths (0.015-0.05 Hz, VLFO). The relevance of this differentiation was unknown and uninvestigated. This is of interest, for one as in the last years multiple fMRI Projects (see Table 3 and 4) have successfully investigated resting state connectivity in the human with fMRI in both healthy subjects and patients with many types of diseases. In contrast, the origin is uncertain, the pathophysiology unclear and the bandwidths and terminology confusing.

In the present studies, we found that two independent bandwidths of functional connectivity coexist. This finding is in line with knowledge from previous research, concerning M- and B-waves. These are of cerebral vascular or neurovascular brainstem origin, respectively. On the other hand, we found no noticeable difference between temporal and spectral measures or also the amount of connectivity between homologous motor cortices. Thus, although we found two independent vascular signals confined to functionally related areas, we found no further evidence for a spatial or functional dissociation. One limitation of this study is the number of participants, leaving the possibility that the lack of dissociation is due to a lack of statistical power. These studies could confirm future fMRI studies of resting state connectivity might need to account for two bandwidths. This has pathophysiological

as well as statistical relevance. The presented results also support the notion that spectral approaches will prove to be better situated to investigate these systems and deserve further investigation. This is supported for one by the trend towards stronger results for spectral methods found in this study as well as, perhaps more importantly, the fact that univariate spectral analyses were unfairly compared with multivariate temporal analyses. This is because multivariate spectral approaches have only recently been introduced to the field of functional connectivity and were not readily available at the time of these investigations. Thus, overall it seems plausible to suggest that the event of easily accessible multivariate spectral analyses will prove to be advantageous for future analyses of resting state connectivity.

The other bandwidths (VVLFO, HFO, and HHFO) did not show functional segregation. We found in line with previous results that the VVLFO were correlated to fluctuations at the edge of the parenchyma. This supports the notion that they are derived from movement, and possibly fluctuations found in the sinuus as well as mechanical noise97.

6.2 Coherence and correlation

We hypothesized that the primary motor cortex connectivity might be coherently related to other functional systems, i.e. non motor-regions of the brain at a phase shift unequal zero. We found that both coherence and correlation approaches were applicable. Neither was better than the other was. We found no strong evidence for a phase-lag differentiation of systems (results not depicted, see also Sun 2005).

In 1995, Biswal and colleagues were the first to suggest the depiction of functional connectivity even in the resting brain of the human test subject and a method was introduced to research spontaneous low frequency fluctuations in fMRI. Thus, a long-standing discussion of neurovascular coupling (vs. myogenic origin) was augmented by the description of positive correlation of low frequency fluctuations between functionally connected distant areas within the human brain. It was concluded that “correlation of low frequency fluctuations, which may arise from fluctuations in blood oxygenation or flow, is a manifestation of functional connectivity of the brain”[98], which mandates a neurovascular origin with which multiple systems could be identified (see Table 4). If these oscillations

share a common originator, or even if they co-exist simultaneously, it is a question of how they might be differentiated. One possibility was that they share common phase stable bandwidths with different phase shifts. Our analysis did not identify further functional systems. This suggests that it is not "only" the phase shift but that further parameters determine the differentiation of functional systems (see also [99] and [100-102]).

It is also interesting to note that the univariate spectral analysis was equally effective as a traditional multivariate time domain analysis. This is in line with theoretical comparisons of spectral vs. temporal approaches in the analysis of oscillatory activity. On the other hand, there is no direct proof that LFO's are a continuous oscillatory signal; although it seems plausible in the light of invasive measures in animal or transcranial Doppler and electroencephalographic measures of oscillatory activity in man (see Table 2).

A quantitative measure of connectivity, e.g. for the comparison of the spectral versus the time domain methods, is derived from Biswal's approach: the index of connectivity between the two primary motor cortices is defined by the ROI size and corrected relative to spurious correlations outside of the motor cortices. This algorithm has obvious shortcomings as functional connectivity must be expected in areas of the sensorimotor network outside of the primary motor areas[103], if truly a measure of functional network "connectedness". Further, there is a large intra- and interindividual variance in the size, as well as localization, in all areas except possibly the primary motor areas. In addition, the statistical threshold between methods might also need to be regarded critically[104].

6.3 Methods of analysis/ A gold standard/ Perspectives?

Is there a gold standard for the analysis of functional connectivity? Most important for our approach and fundamental for the initial analysis of fMRI baseline fluctuations were analyses in the time domain. These were initiated by Biswal and colleagues. They filter a time course derived from a seed voxel. As discussed previously many factors are important for adequate digital filtering. Therefore, for example, we can only assume that the cut-off point (fc) of 0.08 was well chosen and know little about the other parameters (see Methods). Further research will help to define these filtering parameters. Especially in context of the Nyquist-Theorem, aliasing and harmonics[105] as well as different bandwidths

of connectivity, it is interesting to note that such little interest has been shown in discussing types of filters and the data acquisition parameters that should be utilized.

However, it is impressive to recognize how many different approaches have been established. The most successful are most likely the standard multivariate time domain analysis and possibly the blind source separation method suggested by Beckmann and colleagues.

Following Biswal's correlative approach in 1997, Biswal and colleagues showed that the independent component, but not principle component, analysis is capable of identifying functional connectivity. Xiong and colleagues suggested a covariance analysis ("clustered-pixels analysis")[60]. In 2001 Lund introduced physiological noise reduction using vessel time-series (sagittal sinus) as covariates of no interest[106]. 2002, brought the introduction of Hierarchal Clustering, with correlations coefficients per frequency component [107] and a SOM (self organizing maps) algorithm[108]. It was argued that (i) the cross-correlation method is sensitive to drifts in the data, (ii) that the use of "seed clusters" is (1) user-biased, and (2) not applicable in cases where pre-supposed ROIs are not known, (iii) that PCA finds principal components that are orthogonal, and contribute a large amount of variance to the data, but fMRI data can violate orthogonality assumptions (iv) and that fuzzy clustering is not necessary in fMRI since clustering which allows implementation of computationally faster algorithms (such as k-means clustering or self-organizing maps) is more efficient[109]. In 2003, Kiviniemi and colleagues modified the initial correlative approach to accommodate a spectral FT baseline detrending[110]. In 2004, Sun and colleagues introduced a multivariate partial coherence analysis [111]. None of these methods has been formally compared. Further, most of these are in-house productions implemented in varying computer environments. Thus, in view of these facts it seems that like the mainstay of publications (see Table 3 and 4), and due to practical reasons, further investigations will remain in the time domain or via blind source algorithms. Alternatively, the author suggests, that from the results found in this dissertation a formal comparison of a multivariate spectral with a multivariate time-domain approach would be of interest.

6.4 Spurious connectivity and methodological considerations?

In general slow variations (as well as the fast variations) of the fMRI signal can be either of physiological or physical origin. The physiological signal of interest and scanner noise are known to be quadratic or linear to the B0 field in high-field MRI, respectively {Parrish, 2000 19 /id}. Thus, both physiological noise and signal are dependent on the field-strength and exceed thermal as well as scanner noise in grey matter. Low-frequency oscillations have been observed in cadavers[112] and phantoms[113]. Yet, these oscillations below 0,0167 Hz are known to be due to scanner instabilities and not motion or physiological noise[114]. Physiological noise was suggested to reflect oscillations due to respiration, cardiac pulsation and residual movement not accounted for by post-hoc rigid body registration. It has been argued that most fMRI research is performed with a sampling rate of 0.3 Hz, which has lead to confusion in regards to effects of under sampled cardiac (~1 Hz) and respiratory cycles (~0.25 Hz). With this sampling rate, a peak around 0.13 Hz, and between 0.03 and 0.02 Hz has been suggested to be a derivative (aliasing) from cardiac and respiratory cycles, respectively[115]. Yet, others have argued that: “Contrary to what is sometimes stated, there is in general no single frequency band into which the aliasing happens”[116]. However, with respect to LFFC, there is a general agreement that aliasing does not substantially confound the analysis after adequate low pass filtering. The strongest argument commonly being the confinement to functionally associated cerebral regions [117-119]. Here we found highly specific functional segregation for both the VLFO and LFO bandwidth, but not the other bandwidths. Thus, in line with previous literature our results do not support the notion of spurious connectivity.

Physiological noise has been suggested to contaminate functional paradigms [120-122]. It is well known that uncontrolled low frequency oscillations can induce temporal autocorrelation in the residual fMRI signal[123]. It has remained relatively unclear how spontaneous oscillations, that are independent of cardiac and respiratory cycles as well as aliasing, might contribute to the intrinsic measure of autocorrelation. The signal to noise will vary with imaging rate and thus the degree of correlation will vary. Therefore, the false positives will often be estimated either too high or likewise too low. For low frequencies, the variance of the difference in means tends to be underestimated. This results in more false positives than expected.

Thus, as we increase the paradigm frequency, the actual variance approaches and slides below the average value, so we will tend to detect fewer and fewer false positives, at some point detecting fewer false positives than expected[124];[125]. This is also the case for typical retrospective methods of realignment and after temporal filtering[126]. Further, non-white noise is structured in space, which makes it difficult to study states of neural activity with BOLD fMRI if the state remains unchanged for more than a minute[127]. The inclusion of confounding physiological effects in a general linear model (GLM) as covariates of no interest, reduces first and higher order autocorrelation as well as non-normality in the residuals, and thereby improves the validity of the drawn inferences. This is especially important when utilizing high field scanners to increase signal to noise ratio[128]. Our results, suggest that physiological effects will not only globally induce higher order autocorrelation, but that these effects can be dependent on at least two specific and functionally relevant spatiotemporal patterns.

7 Conclusions and open questions:

We found independent VLFO and LFO bandwidth. These might correlate with functional measures of autoregulation (B- and C-waves). Here in both TCD and NIRS data the VLFO bandwidth might be a better measure of autoregulation. In our results, there was a tendency for stronger functional connectivity in this bandwidth. Spectral analyses will be interesting for further investigations of functional connectivity, but it will be important to discard oscillations below 0.167 Hz as they confound the results and are derived from unwanted mechanical or physiological noise. Further, in fMRI variations of autocorrelation due to low frequency oscillations need to be taken into account. More explicitly, it seems very likely that low frequency oscillations will also bias measures of connectivity, e.g. effective connectivity, structural equation modeling or dynamic causal modeling. Thus, the clinical relevance of low frequency connectivity in fMRI deserves further investigation as it is in general an easy and plausibly clinically relevant measure of cerebral function. One next step in this direction might be simultaneous recordings with NIRS and fMRI.

Reference List

1. Davies, P. W. & Bronk, D. W. Oxygen tension in mammalian brain. *Fed. Proc.* **16**, 689-692 (1957).

2. Clark, J., MISRAHY, G. & FOX, R. P. Chronically implanted polarographic electrodes. *J. Appl. Physiol.* **13**, 85-91 (1958).

3. Cooper, R., Crow, H. J., Walter, W. G. & Winter, A. L. Regional control of cerebral vascular reactivity and oxygen supply in man. *Brain Res.* **3**, 174-191 (1966).

4. Halsey Jr, J. H. & McFarland, S. Oxygen cycles and metabolic autoregulation. *Stroke* **5**, 219-225 (1974).

5. Moskalenko, Y. E., Demchenko, I. T., Krivchenko, A. I. & Fedulova, I. P. Dynamics and control mechanisms in maintenance of regional cerebral blood flow. *Stroke* **5**, 461-469 (1974).

6. Manil, J. *et al.* Properties of the spontaneous fluctuations in cortical oxygen pressure. *Adv. Exp. Med. Biol.* **169**, 231-239 (1984).

7. Dora, E. & Kovach, A. G. B. Metabolic and vascular volume oscillations in the cat brain cortex. *Acta Physiologica Academiae Scientiarum Hungaricae* **57**, 261-275 (1981).

8. Vern, B. A., Schuette, W. H., Leheta, B., Juel, V. C. & Radulovacki, M. Low-frequency oscillations of cortical oxidative metabolism in waking and sleep. *J Cereb. Blood Flow Metab* **8**, 215-226 (1988).

9. Hudetz, A. G., Roman, R. J. & Harder, D. R. Spontaneous flow oscillations in the cerebral cortex during acute changes in mean arterial pressure. *J Cereb. Blood Flow Metab* **12**, 491-499 (1992).

10. Golanov, E. V., Yamamoto, S. & Reis, D. J. Spontaneous waves of cerebral blood flow associated with a pattern of electrocortical activity. *Am. J Physiol* **266**, R204-R214 (1994).

11. Mayhew, J. E. *et al.* Cerebral vasomotion: a 0.1-Hz oscillation in reflected light imaging of neural activity. *Neuroimage.* **4**, 183-193 (1996).

12. Rosenblum, B. R., Bonner, R. F. & Oldfield, E. H. Intraoperative measurement of cortical blood flow adjacent to cerebral AVM using laser Doppler velocimetry. *Journal of Neurosurgery* **66**, 396-399 (1987).

13. Fasano, V. A., Urciuoli, R., Bolognese, P. & Mostert, M. Intraoperative use of Laser Doppler in the study of cerebral microvascular circulation. *Acta Neurochirurgica* **95**, 40-48 (1988).

14. Mayhew, J. E. *et al.* Cerebral vasomotion: a 0.1-Hz oscillation in reflected light imaging of neural activity. *Neuroimage.* **4**, 183-193 (1996).

15. Obrig, H. *et al.* Spontaneous low frequency oscillations of cerebral hemodynamics and metabolism in human adults. *Neuroimage.* **12**, 623-639 (2000).

16. Biswal, B., Yetkin, F. Z., Haughton, V. M. & Hyde, J. S. Functional connectivity in the motor cortex of resting human brain using echo-planar MRI. *Magn Reson. Med.* **34**, 537-541 (1995).

17. Moskalenko, Y. E., Cooper, R., Crow, H. J. & WALTER, G. VARIATIONS IN BLOOD VOLUME AND OXYGEN AVAILABILITY IN THE HUMAN BRAIN. *Nature* **202**, 159-161 (1964).

18. Hudetz, A. G., Biswal, B. B., Shen, H., Lauer, K. K. & Kampine, J. P. Spontaneous fluctuations in cerebral oxygen supply. An introduction. *Adv. Exp. Med. Biol.* **454**, 551-559 (1998).

19. Heeger, D. J. & Ress, D. What does fMRI tell us about neuronal activity? *Nat Rev Neurosci* **3**, 142-151 (2002).

20. Nir, Y., Hasson, U., Levy, I., Yeshurun, Y. & Malach, R. Widespread functional connectivity and fMRI fluctuations in human visual cortex in the absence of visual stimulation. *Neuroimage.* **30**, 1313-1324 (2006).

21. Gilden, D. L., Thornton, T. & Mallon, M. W. 1/f noise in human cognition. *Science* **267**, 1837-1839 (1995).

22. Leopold, D. A., Murayama, Y. & Logothetis, N. K. Very Slow Activity Fluctuations in Monkey Visual Cortex: Implications for Functional Brain Imaging. *Cereb. Cortex* **13**, 422-433 (2003).

23. Cooper, R., Crow, H. J., Walter, W. G. & Winter, A. L. Regional control of cerebral vascular reactivity and oxygen supply in man. *Brain Res.* **3**, 174-191 (1966).

24. Moskalenko, Y. E., Cooper, R., Crow, H. J. & WALTER, G. VARIATIONS IN BLOOD VOLUME AND OXYGEN AVAILABILITY IN THE HUMAN BRAIN. *Nature* **202**, 159-161 (1964).

25. Bayliss, W. M. On the local reactions of the arterial wall to changes of internal pressure. *J Physiol* **28**, 220-231 (1902).

26. Cooper, R., Crow, H. J., Walter, W. G. & Winter, A. L. Regional control of cerebral vascular reactivity and oxygen supply in man. *Brain Res.* **3**, 174-191 (1966).

27. Moskalenko, Y. E., Cooper, R., Crow, H. J. & WALTER, G. VARIATIONS IN BLOOD VOLUME AND OXYGEN AVAILABILITY IN THE HUMAN BRAIN. *Nature* **202**, 159-161 (1964).

28. Moskalenko, Y. & Weinstein, G. B. Development of current concepts of physiology of cerebral circulation: A comparative analysis. *Journal of Evolutionary Biochemistry and Physiology* **37**, 492-506 (2001).

29. Vern, B. A. *et al.* Slow oscillations of cytochrome oxidase redox state and blood volume in unanesthetized cat and rabbit cortex. Interhemispheric synchrony. *Adv. Exp. Med. Biol.* **454**, 561-570 (1998).

30. Cooper, R., Crow, H. J., Walter, W. G. & Winter, A. L. Regional control of cerebral vascular reactivity and oxygen supply in man. *Brain Res.* **3**, 174-191 (1966).

31. Cooper, R., Crow, H. J., Walter, W. G. & Winter, A. L. Regional control of cerebral vascular reactivity and oxygen supply in man. *Brain Res.* **3**, 174-191 (1966).

32. Auer, L. M. & Gallhofer, B. Rhythmic activity of cat pial vessels in vivo. *Eur. Neurol.* **20**, 448-468 (1981).

33. Dirnagl, U., Lindauer, U. & Villringer, A. Nitric oxide synthase blockade enhances vasomotion in the cerebral microcirculation of anesthetized rats. *Microvascular Research* **45**, 318-323 (1993).

34. Hudetz, A. G., Roman, R. J. & Harder, D. R. Spontaneous flow oscillations in the cerebral cortex during acute changes in mean arterial pressure. *J Cereb. Blood Flow Metab* **12**, 491-499 (1992).

35. LUNDBERG, N. Continuous recording and control of ventricular fluid pressure in neurosurgical practice. *Acta Psychiatr. Scand. Suppl* **36**, 1-193 (1960).

36. Stephensen, H. *et al.* Objective B wave analysis in 55 patients with non-communicating and communicating hydrocephalus. *J Neurol Neurosurg Psychiatry* **76**, 965-970 (2005).

37. Venes, J. L. B waves--a reflection of cardiorespiratory or cerebral nervous systems rhythm? *Childs Brain* **5**, 352-360 (1979).

38. Rosner, M. J. & Becker, D. P. Origin and evolution of plateau waves. Experimental observations and a theoretical model. *J Neurosurg* **60**, 312-324 (1984).

39. Magnaes, B. Body position and cerebrospinal fluid pressure. Part 1: clinical studies on the effect of rapid postural changes. *J Neurosurg* **44**, 687-697 (1976).

40. Crockard, H. A., Hanlon, K., Duda, E. E. & Mullan, J. F. Hydrocephalus as a cause of dementia: evaluation by computerised tomography and intracranial pressure monitoring. *J Neurol Neurosurg Psychiatry* **40**, 736-740 (1977).

41. Cardoso, E. R., Piatek, D., Del Bigio, M. R., Stambrook, M. & Sutherland, J. B. Quantification of abnormal intracranial pressure waves and isotope cisternography

for diagnosis of occult communicating hydrocephalus. *Surg. Neurol* **31**, 20-27 (1989).

42. Mautner-Huppert, D. *et al.* B-waves in healthy persons. *Neurol Res.* **11**, 194-196 (1989).

43. Einhaupl, K., Garner, C., Dirnagl, U. & et al *Intracranial pressure VI.* Miller, JD., Teasdale, G., Rowan, J., Galbraith, S. & Mendelow, A. (eds.), pp. 290-297 (Springer-Verlag, Berlin Heidelberg,1986).

44. Magnaes, B. Body position and cerebrospinal fluid pressure. Part 1: clinical studies on the effect of rapid postural changes. *J Neurosurg* **44**, 687-697 (1976).

45. Rosner, M. J. & Becker, D. P. Origin and evolution of plateau waves. Experimental observations and a theoretical model. *J Neurosurg* **60**, 312-324 (1984).

46. Steiner, L. A. & Andrews, P. J. Monitoring the injured brain: ICP and CBF. *Br. J Anaesth.* **97**, 26-38 (2006).

47. Mautner-Huppert, D. *et al.* B-waves in healthy persons. *Neurol Res.* **11**, 194-196 (1989).

48. Newell, D. W., Aaslid, R., Stooss, R. & Reulen, H. J. The relationship of blood flow velocity fluctuations to intracranial pressure B waves. *J Neurosurg* **76**, 415-421 (1992).

49. Dearden, N. M. & Midgley, S. Technical Considerations in Continuous Jugular Venous Oxygen-Saturation Measurement. *Acta Neurochirurgica* 91-97 (1993).

50. Beckmann, C. F., DeLuca, M., Devlin, J. T. & Smith, S. M. Investigations into resting-state connectivity using independent component analysis. *Philos. Trans. R. Soc. Lond B Biol. Sci.* **360**, 1001-1013 (2005).

51. Biswal, B., Yetkin, F. Z., Haughton, V. M. & Hyde, J. S. Functional connectivity in the motor cortex of resting human brain using echo-planar MRI. *Magn Reson. Med.* **34**, 537-541 (1995).

52. Cordes, D. *et al.* Mapping functionally related regions of brain with functional connectivity MR imaging. *AJNR Am. J. Neuroradiol.* **21**, 1636-1644 (2000).

53. Cordes, D. *et al.* Frequencies contributing to functional connectivity in the cerebral cortex in "resting-state" data. *AJNR Am. J. Neuroradiol.* **22**, 1326-1333 (2001).

54. Rombouts, S. A., Stam, C. J., Kuijer, J. P., Scheltens, P. & Barkhof, F. Identifying confounds to increase specificity during a "no task condition". Evidence for hippocampal connectivity using fMRI. *Neuroimage.* **20**, 1236-1245 (2003).

55. Strik, C., Klose, U., Kiefer, C. & Grodd, W. Slow rhythmic oscillations in intracranial CSF and blood flow: registered by MRI. *Acta Neurochir. Suppl* **81**, 139-142 (2002).

56. Beckmann, C. F., DeLuca, M., Devlin, J. T. & Smith, S. M. Investigations into resting-state connectivity using independent component analysis. *Philos. Trans. R. Soc. Lond B Biol. Sci.* **360**, 1001-1013 (2005).

57. Lowe, M. J., Mock, B. J. & Sorenson, J. A. Functional connectivity in single and multislice echoplanar imaging using resting-state fluctuations. *Neuroimage.* **7**, 119-132 (1998).

58. Beckmann, C. F., DeLuca, M., Devlin, J. T. & Smith, S. M. Investigations into resting-state connectivity using independent component analysis. *Philos. Trans. R. Soc. Lond B Biol. Sci.* **360**, 1001-1013 (2005).

59. Salvador, R., Suckling, J., Schwarzbauer, C. & Bullmore, E. Undirected graphs of frequency-dependent functional connectivity in whole brain networks. *Philos. Trans. R. Soc. Lond B Biol. Sci.* **360**, 937-946 (2005).

60. Xiong, J., Parsons, L. M., Gao, J. H. & Fox, P. T. Interregional connectivity to primary motor cortex revealed using MRI resting state images. *Hum. Brain Mapp.* **8**, 151-156 (1999).

61. Beckmann, C. F., DeLuca, M., Devlin, J. T. & Smith, S. M. Investigations into resting-state connectivity using independent component analysis. *Philos. Trans. R. Soc. Lond B Biol. Sci.* **360**, 1001-1013 (2005).

62. Cordes, D. *et al.* Frequencies contributing to functional connectivity in the cerebral cortex in "resting-state" data. *AJNR Am. J. Neuroradiol.* **22**, 1326-1333 (2001).

63. Cordes, D. *et al.* Frequencies contributing to functional connectivity in the cerebral cortex in "resting-state" data. *AJNR Am. J. Neuroradiol.* **22**, 1326-1333 (2001).

64. Strik, C., Klose, U., Erb, M., Strik, H. & Grodd, W. Intracranial oscillations of cerebrospinal fluid and blood flows: analysis with magnetic resonance imaging. *J. Magn Reson. Imaging* **15**, 251-258 (2002).

65. De, L. M., Beckmann, C. F., De, S. N., Matthews, P. M. & Smith, S. M. fMRI resting state networks define distinct modes of long-distance interactions in the human brain. *Neuroimage.* **29**, 1359-1367 (2006).

66. Beckmann, C. F., DeLuca, M., Devlin, J. T. & Smith, S. M. Investigations into resting-state connectivity using independent component analysis. *Philos. Trans. R. Soc. Lond B Biol. Sci.* **360**, 1001-1013 (2005).

67. Obrig, H. *et al.* Spontaneous low frequency oscillations of cerebral hemodynamics and metabolism in human adults. *Neuroimage.* **12**, 623-639 (2000).

68. Biswal, B., Yetkin, F. Z., Haughton, V. M. & Hyde, J. S. Functional connectivity in the motor cortex of resting human brain using echo-planar MRI. *Magn Reson. Med.* **34**, 537-541 (1995).

69. Obrig, H. *et al.* Spontaneous low frequency oscillations of cerebral hemodynamics and metabolism in human adults. *Neuroimage.* **12**, 623-639 (2000).

70. Obrig, H. *et al.* Spontaneous low frequency oscillations of cerebral hemodynamics and metabolism in human adults. *Neuroimage.* **12**, 623-639 (2000).

71. Obrig, H. *et al.* Spontaneous low frequency oscillations of cerebral hemodynamics and metabolism in human adults. *Neuroimage.* **12**, 623-639 (2000).

72. Roy, C. S. & Sherrington, C. S. On the Regulation of the Blood-supply of the Brain. *J Physiol* **11**, 85-158 (1890).

73. Bandettini, P. A., Wong, E. C., Hinks, R. S., TIkofsky, R. S. & Hyde, J. S. Time course EPI of human brain function during task activation. *Magn. Reson. Med.* **25**, 390 (1992).

74. Kwong, K. K., Belliveau, J. W., Chesler, D. A., Goldberg, I. E. & Weiskoff, R. M. Dynamic magnetic resonance imaging of human brain activity during primary sensory stimulation. *Proc. Natl. Acad. Sci. USA* **89**, 5675 (1992).

75. Mitra, P. P., Ogawa, S., Hu, X. & Ugurbil, K. The nature of spatiotemporal changes in cerebral hemodynamics as manifested in functional magnetic resonance imaging. *Magn Reson. Med.* **37**, 511-518 (1997).

76. Mitra, P. P., Ogawa, S., Hu, X. & Ugurbil, K. The nature of spatiotemporal changes in cerebral hemodynamics as manifested in functional magnetic resonance imaging. *Magn Reson. Med.* **37**, 511-518 (1997).

77. Ogawa, S., Lee, T. M., Kay, A. R. & Tank, D. W. Brain magnetic resonance imaging with contrast dependent on blood oxygenation. *Proc. Natl Acad. Sci. U. S. A* **87**, 9868-9872 (1990).

78. Friston, K. J., Frith, C. D., Frackowiak, R. S. & Turner, R. Characterizing dynamic brain responses with fMRI: a multivariate approach. *Neuroimage.* **2**, 166-172 (1995).

79. Friston, K. J., Frith, C. D., Frackowiak, R. S. & Turner, R. Characterizing dynamic brain responses with fMRI: a multivariate approach. *Neuroimage.* **2**, 166-172 (1995).

80. Smith, S. *The Scientist and Engineer's Guide to Digital Signal Processing*. (1999).

81. Biswal, B., Yetkin, F. Z., Haughton, V. M. & Hyde, J. S. Functional connectivity in the motor cortex of resting human brain using echo-planar MRI. *Magn Reson. Med.* **34**, 537-541 (1995).

82. Biswal, B., DeYoe, A. E. & Hyde, J. S. Reduction of physiological fluctuations in fMRI using digital filters. *Magn Reson. Med.* **35**, 107-113 (1996).

83. Biswal, B., Yetkin, F. Z., Haughton, V. M. & Hyde, J. S. Functional connectivity in the motor cortex of resting human brain using echo-planar MRI. *Magn Reson. Med.* **34**, 537-541 (1995).

84. Obrig, H. *et al.* Spontaneous low frequency oscillations of cerebral hemodynamics and metabolism in human adults. *Neuroimage.* **12**, 623-639 (2000).

85. Muthuswamy, J. & Thakor, N. V. Spectral analysis methods for neurological signals. *J Neurosci Methods* **83**, 1-14 (1998).

86. Muthuswamy, J. & Thakor, N. V. Spectral analysis methods for neurological signals. *J Neurosci Methods* **83**, 1-14 (1998).

87. Yousry, T. A. *et al.* Localization of the motor hand area to a knob on the precentral gyrus. A new landmark. *Brain* **120 (Pt 1)**, 141-157 (1997).

88. Yousry, T. *et al.* [The motor hand area. Noninvasive detection with functional MRI and surgical validation with cortical stimulation]. *Radiologe* **35**, 252-255 (1995).

89. Yousry, I., Naidich, T. P. & Yousry, T. A. Functional magnetic resonance imaging: factors modulating the cortical activation pattern of the motor system. *Neuroimaging Clin. N. Am.* **11**, 195-202, viii (2001).

90. Smith, A. M. *et al.* Investigation of low frequency drift in fMRI signal. *Neuroimage.* **9**, 526-533 (1999).

91. Smith, A. M. *et al.* Investigation of low frequency drift in fMRI signal. *Neuroimage.* **9**, 526-533 (1999).

92. Mayhew, J. E. *et al.* Cerebral vasomotion: a 0.1-Hz oscillation in reflected light imaging of neural activity. *Neuroimage.* **4**, 183-193 (1996).

93. Talairach, J. & Tournoux, R. *Co-Planar Steriotaxic Atlas of the Human Brain*. Thieme, Stuttgart (1988).

94. Yousry, T. *et al.* [The motor hand area. Noninvasive detection with functional MRI and surgical validation with cortical stimulation]. *Radiologe* **35**, 252-255 (1995).

95. Yousry, T. *et al.* [The motor hand area. Noninvasive detection with functional MRI and surgical validation with cortical stimulation]. *Radiologe* **35**, 252-255 (1995).

96. Biswal, B., Yetkin, F. Z., Haughton, V. M. & Hyde, J. S. Functional connectivity in the motor cortex of resting human brain using echo-planar MRI. *Magn Reson. Med.* **34**, 537-541 (1995).

97. Smith, A. M. *et al.* Investigation of low frequency drift in fMRI signal. *Neuroimage.* **9**, 526-533 (1999).

98. Biswal, B., Yetkin, F. Z., Haughton, V. M. & Hyde, J. S. Functional connectivity in the motor cortex of resting human brain using echo-planar MRI. *Magn Reson. Med.* **34**, 537-541 (1995).

99. Obrig, H. *et al.* Spontaneous low frequency oscillations of cerebral hemodynamics and metabolism in human adults. *Neuroimage.* **12**, 623-639 (2000).

100. Sun, F. T., Miller, L. M. & D'Esposito, M. Measuring temporal dynamics of functional networks using phase spectrum of fMRI data. *NeuroImage* **28**, 227-237 (2005).

101. Mitra, P. P., Ogawa, S., Hu, X. & Ugurbil, K. The nature of spatiotemporal changes in cerebral hemodynamics as manifested in functional magnetic resonance imaging. *Magn Reson. Med.* **37**, 511-518 (1997).

102. Cordes, D. *et al.* Frequencies contributing to functional connectivity in the cerebral cortex in "resting-state" data. *AJNR Am. J. Neuroradiol.* **22**, 1326-1333 (2001).

103. Bestmann, S., Baudewig, J., Siebner, H. R., Rothwell, J. C. & Frahm, J. Subthreshold high-frequency TMS of human primary motor cortex modulates interconnected frontal motor areas as detected by interleaved fMRI-TMS. *NeuroImage* **20**, 1685-1696 (2003).

104. Mayhew, J. E. *et al.* Cerebral vasomotion: a 0.1-Hz oscillation in reflected light imaging of neural activity. *Neuroimage.* **4**, 183-193 (1996).

105. Lund, T. E. fcMRI--mapping functional connectivity or correlating cardiac-induced noise? *Magn Reson. Med.* **46**, 628-629 (2001).

106. Lund, T. E. fcMRI--mapping functional connectivity or correlating cardiac-induced noise? *Magn Reson. Med.* **46**, 628-629 (2001).

107. Cordes, D. *et al.* Mapping functionally related regions of brain with functional connectivity MR imaging. *AJNR Am. J. Neuroradiol.* **21**, 1636-1644 (2000).

108. Peltier, S. J., Polk, T. A. & Noll, D. C. Detecting low-frequency functional connectivity in fMRI using a self-organizing map (SOM) algorithm. *Hum. Brain Mapp.* **20**, 220-226 (2003).

109. Peltier, S. J., Polk, T. A. & Noll, D. C. Detecting low-frequency functional connectivity in fMRI using a self-organizing map (SOM) algorithm. *Hum. Brain Mapp.* **20**, 220-226 (2003).

110. Kiviniemi, V. *et al.* Slow vasomotor fluctuation in fMRI of anesthetized child brain. *Magn Reson. Med.* **44**, 373-378 (2000).

111. Sun, F. T., Miller, L. M. & D'Esposito, M. Measuring temporal dynamics of functional networks using phase spectrum of fMRI data. *NeuroImage* **28**, 227-237 (2005).

112. Smith, A. M. *et al.* Investigation of low frequency drift in fMRI signal. *Neuroimage.* **9**, 526-533 (1999).

113. Lund, T. E. fcMRI--mapping functional connectivity or correlating cardiac-induced noise? *Magn Reson. Med.* **46**, 628-629 (2001).

114. Smith, A. M. *et al.* Investigation of low frequency drift in fMRI signal. *Neuroimage.* **9**, 526-533 (1999).

115. Beckmann, C. F., DeLuca, M., Devlin, J. T. & Smith, S. M. Investigations into resting-state connectivity using independent component analysis. *Philos. Trans. R. Soc. Lond B Biol. Sci.* **360**, 1001-1013 (2005).

116. Kruger, G. & Glover, G. H. Physiological noise in oxygenation-sensitive magnetic resonance imaging. *Magn Reson. Med.* **46**, 631-637 (2001).

117. Lowe, M. J., Mock, B. J. & Sorenson, J. A. Functional connectivity in single and multislice echoplanar imaging using resting-state fluctuations. *Neuroimage.* **7**, 119-132 (1998).

118. Biswal, B., Yetkin, F. Z., Haughton, V. M. & Hyde, J. S. Functional connectivity in the motor cortex of resting human brain using echo-planar MRI. *Magn Reson. Med.* **34**, 537-541 (1995).

119. Stein, T. *et al.* Functional connectivity in the thalamus and hippocampus studied with functional MR imaging. *AJNR Am. J. Neuroradiol.* **21**, 1397-1401 (2000).

120. Obrig, H. *et al.* Spontaneous low frequency oscillations of cerebral hemodynamics and metabolism in human adults. *Neuroimage.* **12**, 623-639 (2000).

121. Nir, Y., Hasson, U., Levy, I., Yeshurun, Y. & Malach, R. Widespread functional connectivity and fMRI fluctuations in human visual cortex in the absence of visual stimulation. *Neuroimage.* **30**, 1313-1324 (2006).

122. Leopold, D. A., Murayama, Y. & Logothetis, N. K. Very Slow Activity Fluctuations in Monkey Visual Cortex: Implications for Functional Brain Imaging. *Cereb. Cortex* **13**, 422-433 (2003).

123. Kruger, G. & Glover, G. H. Physiological noise in oxygenation-sensitive magnetic resonance imaging. *Magn Reson. Med.* **46**, 631-637 (2001).

124. Zarahn, E., Aguirre, G. K. & D'Esposito, M. Empirical analyses of BOLD fMRI statistics. I. Spatially unsmoothed data collected under null-hypothesis conditions. *Neuroimage.* **5**, 179-197 (1997).

125. Purdon, P. L. & Weisskoff, R. M. Effect of temporal autocorrelation due to physiological noise and stimulus paradigm on voxel-level false-positive rates in fMRI. *Hum. Brain Mapp.* **6**, 239-249 (1998).

126. Lowe, M. J., Mock, B. J. & Sorenson, J. A. Functional connectivity in single and multislice echoplanar imaging using resting-state fluctuations. *Neuroimage.* **7**, 119-132 (1998).

127. Dagli, M. S., Ingeholm, J. E. & Haxby, J. V. Localization of cardiac-induced signal change in fMRI. *NeuroImage* **9**, 407-415 (1999).

128. Kruger, G. & Glover, G. H. Physiological noise in oxygenation-sensitive magnetic resonance imaging. *Magn Reson. Med.* **46**, 631-637 (2001).

Erklärung / Declaration

„Ich, Sein, Schmidt, erkläre, dass ich die vorgelegte Dissertationsschrift mit dem Thema: *Bandwidth-Specific Functional Connectivity of Physiological Low Frequency Oscillations in fMRI* selbst verfasst und keine anderen als die angegebenen Quellen und Hilfsmittel benutzt, ohne die (unzulässige) Hilfe Dritter verfasst und auch in Teilen keine Kopien anderer Arbeiten dargestellt habe."

"I, Sein Schmidt, declare that I submitted the dissertation with the theme: *Bandwidth-Specific Functional Connectivity of Physiological Low Frequency Oscillations in fMRI*, and drafted it with no other than the specified sources and tools without the (illegal) assistance of a Third party or copies in part from other works."

Date Signature

Mein Lebenslauf wird aus datenschutzrechtlichen Gründen in der elektronischen Version meiner Arbeit nicht veröffentlicht.